geosciences

MDPI

Article

Safety Assessment of Concrete Gravity Dams: Hydromechanical Coupling and Fracture Propagation

Maria Luísa Braga Farinha *, Nuno Monteiro Azevedo and Sérgio Oliveira

Concrete Dams Department, National Laboratory for Civil Engineering (LNEC), 1700-066 Lisboa, Portugal; nazevedo@lnec.pt (N.M.A.); soliveira@lnec.pt (S.O.)

* Correspondence: lbraga@lnec.pt; Tel.: +351-218443375

Abstract: For the safety assessment of concrete dam–foundation systems, this study used an explicit time-stepping small-displacement algorithm, which simulates the hydromechanical interaction and considers the discrete representation of the foundation discontinuities. The proposed innovative methodology allows for the definition of more reliable safety factors and the identification of more realistic failure modes by integrating (i) softening-based constitutive laws that are closer to the real behavior identified experimentally in concrete–concrete and concrete–rock interfaces; (ii) a water height increase that can be considered in both hydraulic and mechanical models; and (iii) fracture propagation along the dam–foundation interface. Parametric studies were conducted to assess the impact of the mechanical properties on the global safety factors of three gravity dams with different heights. The results obtained using a coupled/fracture propagation model were compared with those from the strength reduction method and the overtopping scenario not considering the hydraulic pressure increase. The results show that the safety assessment should be conducted using the proposed methodology. It is shown that the concrete–rock interface should preferably have a high value of fracture energy or, ideally, higher tensile and cohesion strengths and high associated fracture energy. The results also indicate that with a brittle concrete–rock model, the predicted safety factors are always conservative when compared with those that consider the fracture energy.

Keywords: concrete gravity dams; safety assessment; overtopping; discrete hydromechanical coupled model; fracture propagation

Academic Editors: Wenfeng Li and Shahrzad Roshankhah

Received: 14 February 2025
Revised: 4 April 2025
Accepted: 13 April 2025
Published: 15 April 2025

Citation: Farinha, M.L.B.; Azevedo, N.M.; Oliveira, S. Safety Assessment of Concrete Gravity Dams: Hydromechanical Coupling and Fracture Propagation. *Geosciences* **2025**, *15*, 149. https://doi.org/10.3390/geosciences15040149

1. Introduction

Dams still present an intrinsic risk to development, with accidents remaining a significant concern today [1]. Therefore, given the potential of material and human losses associated with dam failure, it is mandatory to adopt a framework that has the capacity to anticipate and prevent failures. The current approaches based on simplified limit equilibrium techniques [2,3] are not able to characterize the complex dam–foundation behavior. The ability to evaluate the safety of dam–foundation systems in an integrated manner requires further enhancement, particularly by incorporating coupled models that capture the significant interdependence between the mechanical and hydraulic behaviors [4,5]. Additionally, the use of appropriate constitutive laws is essential [6–10].

For the analysis of gravity dams, fully coupled two-dimensional (2D) and three-dimensional discontinuum hydromechanical models have been used [11] following sequential coupling. The interpretation of the observed behavior during the first filling of the reservoir [11] should also consider the hydromechanical coupling in both the 2D and

3D models. Similar hydromechanical models to those adopted in dam analysis, based on the combined finite–discrete element method (FDEM), have been proposed in 2D [12] and 3D [13] models for hydraulic rock fracturing. The latter 2D and 3D models have also been extended to include thermal coupling [14,15]. The 3D thermal–hydromechanical coupling model (THM) considers the FDEM fracture mechanic calculation model, fracture–pore mixed seepage model and heat transfer model (heat conduction in solids and fluids, heat advection and heat exchange between solids and fluids) [15]. A 2D FDEM-based THM model that follows the software Geomechanica [16] has also been adopted for hydraulic fracturing in deep reservoirs [17]. More recently, a hydromechanical model has also been established for poroelastic media saturated with compressible fluids, which adopts a strong coupling between the mechanical and hydraulic based on the extended finite element method (XFEM) and the Newton–Raphson method [18]. A 2D hydromechanical coupling model has also been proposed within the framework of discontinuous deformation analysis (DDA) and was applied to evaluate the sliding stability of a gravity dam foundation in China [19]. A hydromechanical continuum model based on the finite element method (FEM) was adopted to analyze the seepage and stress field characteristics of a roller-compacted concrete dam in China [20].

Regarding the simulation of the behavior of the different materials, the discontinuities and the hydromechanical coupling during shear displacement, various constitutive models/relationships have been established over time. The tensile and compressive strength of dam concrete, along with its long-term behavior, have been well characterized through both in situ and laboratory tests, which are typically conducted whenever a new dam is constructed [21,22]. However, the mechanical behavior of the concrete–rock interface—often one of the weakest structural points, prone to crack initiation and propagation under hydrostatic loading—has been less thoroughly studied.

Direct tensile strength tests have been performed on cored concrete–rock specimens [23]. More recently, an experimental program was carried out to investigate the mechanics and fracture properties of the concrete–rock interface, leading to the development of a tension-softening constitutive law for this interface [24]. This experimental program was further extended to examine the fracture process at rock–concrete interfaces under the three-point bending and four-point shearing of rock–concrete composite beams with various pre-crack positions using digital image correlation techniques [25]. More recently, the concrete–granite composite materials were numerically assessed following a mesoscopic approach under compression loads and different interface inclination angles [26].

Concrete gravity and buttress dams are usually assumed to fail along a sliding plane, acting as a rigid body. The stability criteria are commonly assessed for two different failure modes: sliding and overturning failure. The limits for stability are given in national or regional codes and regulations [27]. In most cases, interface cohesion is neglected.

Regarding stability analysis, there are two primary approaches to simulate concrete dam structural failure: (i) strength reduction and (ii) overload. In the strength reduction approach, the structure is subjected to normal loads, and its strength is gradually decreased until failure happens. In the overload approach, normal loads are applied to the structure, and these loads are progressively increased until the structure fails [28]. At the design stage, concrete gravity dam safety assessments are usually based on simplified analytical stability methods [27,29] performed in 2D with a simplified rock surface. The European Working Group on the sliding safety of existing gravity dams addressed in its final report [30] guidelines, site data information, experimental programs, safety assessment techniques and three-dimensional effects.

Li et al. [31] evaluated the stability of a large gravity dam using both the overload and strength reduction methods, but the pressures followed simplified analytical distributions. These authors highlight that the overload method, which includes more complex geometries, can be adopted to define the weak structural interfaces/zones that may require reinforcement measures. The strength reduction may also be more complex by reducing both the cohesion and friction angle. In [32], a reduction model based on a plastic strain energy-based criterion is proposed for the bed rock and weak foundation zones. Note that the latter does not include seepage water pressures. Stability analysis has also been addressed through probabilistic analysis, usually adopting simple models or analytical expressions due to computational issues but considering uncertainties in the structural analysis and their influence on the safety factors [33–35]. Within this methodology, it is still computationally demanding to consider the hydromechanical coupling.

Although numerical modeling techniques have been widely used to simulate the failure of concrete dams, mostly the FEM [36] and the discrete element method (DEM), testing programs are still devised to confirm the reliability of the application of the numerical models to the study of failure mechanisms that involve sliding in jointed rock masses by comparing numerical results with experimental data, in both static and dynamic conditions. Most of the tests are carried out under overloading conditions [37,38]. Enzell et al. [37] developed a 25 m long prototype of a concrete buttress dam. The testing involved gradually increasing the water pressure until the model failed. Initially, a watertight steel sheet wall was placed upstream of the dam to allow the water level to rise above the dam's crest, transmitting water pressures to both the dam and its foundation without causing overtopping. In the numerical study presented here, this setup was precisely simulated. The steel sheet was subsequently removed to permit overtopping.

In this study, the Parmac2D-Fflow algorithm, which uses a time-stepping small-displacement hydromechanical coupled approach, including the discrete representation of the foundation discontinuities, was employed to assess the safety of gravity dams [39,40]. Compared with the strength reduction approach or the overtopping approach without hydromechanical coupling, the proposed innovative methodology has the advantage of allowing the consideration, in an integrated way, of (i) softening-based constitutive laws that are closer to the real behavior identified experimentally in concrete–concrete and concrete–rock interfaces; (ii) the influence of the water height increase on both the hydraulic and mechanical models; and (iii) fracture propagation along the dam–foundation interface, only allowing seepage to occur when the interface is cracked, which is closer to the expected behavior given the way that this interface is constructed. As shown, the proposed innovative methodology for the safety assessment of concrete dams allows for the definition of more reliable safety factors and the identification of more realistic failure modes that may be strengthened following retrofitting interventions. Within dam engineering, more realistic numerical constitutive models have been adopted mainly for concrete [41].

Parametric studies were conducted to assess the impact of the mechanical properties, namely, the concrete–rock strength parameters, on the global safety factors of three gravity dams with different heights, foundation behaviors and geometries. The results obtained using a coupled/fracture propagation model, including those for which the water height increase had an influence on the water pressures, are compared with those from the strength reduction method and the overtopping scenario not considering the hydromechanical coupling as the water height is increased.

The results show that the safety assessment should be conducted using a coupled hydromechanical model that incorporates accurate material properties, namely, for the concrete–rock interface, and that considers the foundation geometry and behavior close to the in situ conditions and follows a load amplification approach that can identify weak

structural zones. It is shown that the concrete–rock interface should preferably have a high value of fracture energy or, ideally, higher tensile and cohesion strengths and high associated fracture energy. The results also indicate that with a brittle concrete–rock model, the predicted safety factors are always conservative when compared with those that consider the fracture energy.

2. Numerical Approach

2.1. Mechanical Model

The adopted hydromechanical model, Parmac2D-Fflow, allows for the coupling between the hydraulic behavior and the mechanical behavior [42] and is part of the computational model Parmac2D [43]. The Parmac2D-Fflow implementation was chosen for the safety assessment of concrete gravity dams because it represents the foundation discontinuities, which are a key parameter in the safety assessment, and by including joint finite elements, it allows for faster and more accurate modeling when compared with discrete element approaches [42]. The adopted hydromechanical approach [42] and similar hydromechanical models [12,13] have been validated and compared with benchmark tests and with the real behavior of a Portuguese gravity dam. More recently, a similar DEM-based model [44] was used to study the uplift pressure distribution at a dam–foundation interface, showing that the limit equilibrium approach may underestimate the stress magnitude at both the dam heel and toe [45].

The mechanical model follows an explicit solution algorithm based on the centered difference method [43] that calculates the velocities at the mid-intervals ($t \pm \Delta t/2$), while the generalized positions and accelerations are defined at the primary intervals ($t \pm \Delta t$). The deformability of each block is considered by discretizing its interior with a finite element triangular mesh. Newton's second law of motion is integrated twice to define the nodal point displacements, leading to the following expressions for the nodal point velocities at time $t + \Delta t/2$:

$$x_i^{t+\Delta t/2} = x_i^{t-\Delta t/2} + \frac{F_i(t) + F_i^d(t)}{m}\Delta t \quad (1)$$

where $F_i(t)$ is the total applied force at instant t, $F_i^d(t)$ is the damping force at instant t, m is the nodal point mass, $x_i^{t+\Delta t/2}$ represents the velocity vector at time $t + \Delta t/2$, and $x_i^{t-\Delta t/2}$ represents the velocity vector at time $t - \Delta t/2$. The total applied forces are due to (i) the external forces applied at the nodal point; (ii) the interactions with neighboring blocks, which only occur at nodal points located at the block boundaries; and (iii) the deformation of the inner block triangular finite elements.

The interaction between deformable blocks is carried out using joint finite elements (FEs) [46,47] that require (i) a small-displacement hypothesis; (ii) that each block's finite element boundary discretization is compatible with the boundary finite element discretization of the neighboring blocks. When compared with the DEM, which handles large displacements [42], the FEM-based joint element approach makes it easier to incorporate nonlinear elastoplastic and damage models. The discrete block foundation geometry was defined using UDEC [44,48]. A pre-processing stage is applied to obtain a perfectly compatible final block assembly with joint elements (see [42] for more details).

The FE-based joint element allows for discontinuity in the displacement field using a direct relation between the stresses and displacements. At each joint element integration point, the normal $\sigma_n(t + \Delta t)$ and shear $\tau_s(t + \Delta t)$ stresses in the local axis are given as follows:

$$\sigma_n(t + \Delta t) = \sigma_n(t) + k_n \Delta u_n(t) \quad (2)$$

$$\tau_s(t + \Delta t) = \tau_s(t) + k_s \Delta u_s(t) \quad (3)$$

where $\sigma_n(t)$ and $\tau_s(t)$ are the normal and shear stresses at timestep t; $\Delta u_n(t)$ and $\Delta u_s(t)$ are the displacement increments in both the normal and tangential joint directions; and k_n and k_s are the normal and shear contact stiffnesses.

To represent the concrete–concrete and concrete–rock discontinuity behavior, a bilinear vectorial softening contact model (BL) was adopted, which has been applied in particle modeling fracture studies [43] (Figure 1). As presented in Figure 1, once the maximum strength values (tensile and cohesion strengths) are reached, the corresponding maximum tensile strength and/or maximum cohesion stress are updated based on the updated damage value. The damage value ranges from 0 (no damage) to 1 (the integration point is cracked and only transfers normal and shear stresses through pure friction under normal compression stress).

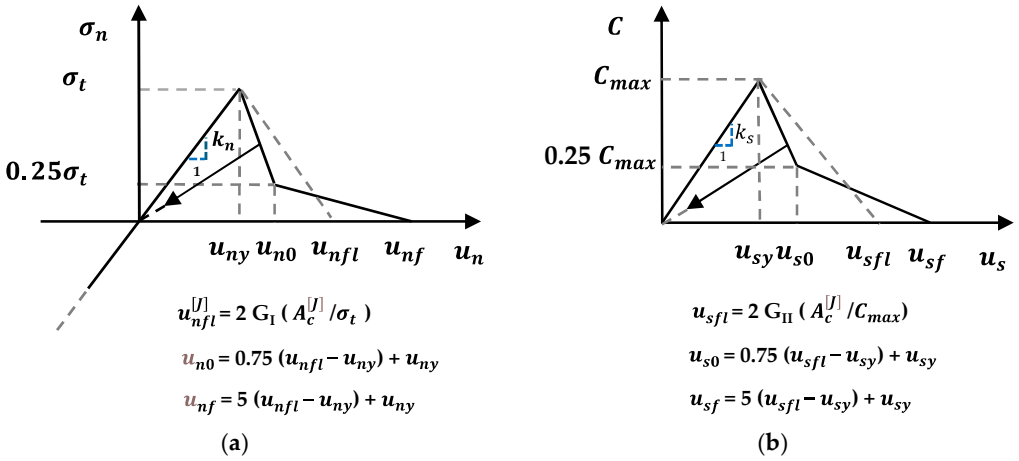

Figure 1. Bilinear vectorial softening contact model (BL): (**a**) normal-tensile direction and (**b**) shear direction ($\tau = C + \sigma_n \mu_c$).

The damage value at each integration point is defined by the greater of the maximum tensile and shear damage values, which are defined given the maximum recorded normal and shear joint displacement values. The constitutive law requires the definition of five material properties: (i) the ultimate tensile stress (σ_t); (ii) the maximum cohesion stress (C_{max}); (iii) the coefficient of friction (μ_c); (iv) the fracture energy in mode I (G_I); and (v) the fracture energy in mode II (G_{II}).

2.2. Hydraulic Model

The hydraulic model is proposed in [42] and is based on the principles defined in [44] for a large-displacement formulation based on the DEM. A similar hydraulic model has been proposed in 2D and applies hydraulic fracture propagation [12]. The hydraulic model has been extensively validated in simple benchmark examples [12,42,44].

Figure 2 shows both the mechanical and hydraulic models. Figure 2a shows the mechanical model, in which four different blocks are represented, discretized with triangular finite elements, along with the corresponding joint elements (JEs). The hydraulic model (Figure 2b) is perfectly superimposed on the mechanical model (Figure 2a) in a straightforward way, given that a perfectly compatible boundary mesh of plane triangular elements was defined during pre-processing [42]. The seepage channels (SCs) of the hydraulic model, shown in Figure 2b, align with the midplane of the joint elements, shown in Figure 2a [42]. For each JE, there is a corresponding seepage channel (SC). The hydraulic nodes (HNs) are the result of the superimposition of the various adjacent mechanical nodes that shared the same coordinates at the beginning of the numerical analysis.

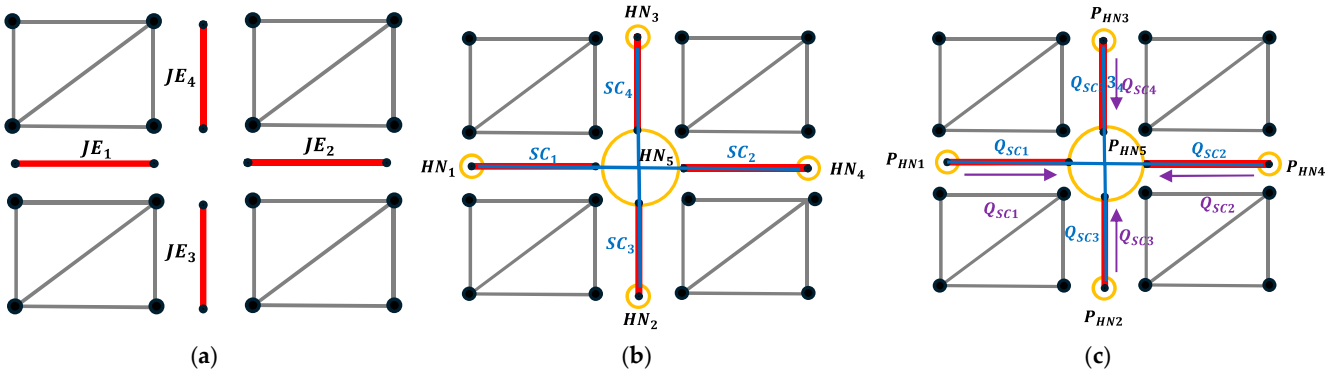

Figure 2. Hydraulic model superimposed on the mechanical model: (**a**) mechanical model: joint elements (JEs) and nodes; (**b**) hydraulic model: hydraulic nodes (HNs) and seepage channels (SCs); (**c**) hydraulic model: pressures (Ps) on the hydraulic nodes and discharges (Qs) in seepage channels.

The volume of each SC is obtained considering the mechanical apertures measured on the nodal points of the JE associated with the SC. It is assumed that flow takes place only through the set of interconnecting discontinuities (rock blocks are impervious).

Water pressures are defined on the HNs, and flow rates are calculated in the SCs (Figure 2c). The discharge rate of each SC is calculated based on the simplified assumption of laminar seepage between parallel plates [49–51]. This discharge rate ($(m^3/s)/m$) is given as follows [52]:

$$Q_{SC} = \frac{1}{12\,\mu} a_{h.SC}^3\, \rho_w\, g \frac{\Delta H_{SC}}{L} = k_{SC} \rho_w\, g\, \Delta H_{SC} \tag{4}$$

where $\frac{1}{12\,\mu}$ is the theoretical value of a joint permeability factor (also called the joint permeability constant), where μ is the dynamic viscosity of the fluid; $a_{h.SC}$ is the hydraulic aperture of the seepage channel; ρ_w is the water density; g is the acceleration of gravity; ΔH_{SC} is the difference in the piezometric head between both ends of the seepage channel; and L is the length of the SC.

In each HN, the discharges are summed from all the seepage channels that converge to a given HN, according to the following:

$$Q_{HN}(\mathrm{t}) = \sum_{i=1}^{n} Q_{SCi}(\mathrm{t}) \tag{5}$$

If only steady-state conditions are considered, the volume variation between two consecutive timesteps may be neglected. The HN water pressure at the following timestep ($P_{HN}(t + \Delta t)$) is given as follows:

$$P_{HN}(t + \Delta t) = P_{HN}(t) + \frac{K_W}{V_{HN}(t)} Q_{HN}(\mathrm{t})\, \Delta t \tag{6}$$

where K_W is the water bulk modulus (N/m^2), $V_{HN}(t)$ is the volume variation (m^3) associated with the HN between two consecutive steps and Δt is the timestep used in the hydraulic domain.

The hydraulic aperture to be used in Equation (4) ($a_{h.SC}$) is given as follows:

$$a_{h.SC} = a_0 + \mathrm{u}_n \tag{7}$$

where a_0 is the hydraulic aperture at nominal zero normal stress, and u_n is the joint normal displacement taken as positive in the opening. As shown in Figure 3, a maximum aperture value, a_{max}, is adopted for numerical convergence issues. A minimum aperture value, a_{min}, is also adopted, below which mechanical closure does not affect the contact permeability (Figure 3) [12,13,42,44].

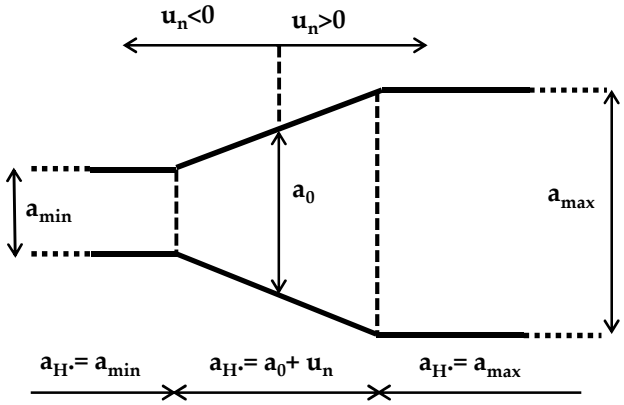

Figure 3. Hydraulic aperture minimum and maximum boundaries given the hydraulic aperture at nominal zero normal stress (a_0) and the mechanical opening (u_n).

Regarding the hydraulic boundary conditions, the HNs may be assumed to have zero permeability, usually adopted at the bottom and lateral faces of the foundation rock mass. The HNs may also have imposed pressure values, which are usually used to set the pressures at the top of the foundation, upstream and downstream from the dam and at the HNs intersected by the drainage system.

A 3D extension that also adopts seepage channels has been proposed for dam foundation hydromechanical analysis [11], and a 3D model that follows a similar methodology but adopts seepage surfaces has been proposed [13] for hydraulic fracture propagation.

2.3. Coupled Hydromechanical Model

A sequential coupling scheme is adopted between the mechanical model and the hydraulic model, which evolves over time through the interaction between both domains. At each timestep, the seepage channel hydraulic apertures are calculated considering the normal displacements of the associated joint elements calculated with the mechanical model. Following this, the water pressures calculated using the hydraulic model are then transferred to the mechanical model and are considered in the calculation of the internal forces of the associated joint elements (effective stresses). Additional details can be found in [42]. Regarding stability issues, the hydraulic volumes associated with the HNs and the masses associated with the mechanical nodal points are scaled assuming a unitary timestep in order to ensure numerical stability [42].

The adopted discontinuum hydromechanical model allows for two different approaches for the seepage flow:

(i) Seepage occurs in all interfaces independently of their damage, and the corresponding water pressures are installed from the beginning of the simulation on all interfaces, including the dam–foundation interface;

(ii) At the dam–foundation interface, seepage only occurs after the joint element integration points are found to be cracked, making it possible to model a coupled propagation failure along the dam–foundation interface due to a hypothetical dam overtopping scenario (CP-FP). An initially impervious dam–foundation interface is a more realistic scenario given the way that the concrete dam is built, as special foundation treatment is carried out to ensure cohesion between the concrete and foundation rock, which significantly reduces the permeability in the absence of fracture.

2.4. Model Geometry

Three gravity dams of different heights, (15 m, 30 m and 60 m) were assessed adopting two foundation fracture geometries. Figure 4 shows the schematic geometry of the adopted dam–foundation system. Table 1 presents all the required geometric parameters to generate

the models. The adopted dam cross-section geometry is within the usual dimensions given the dam height. The grout curtain geometry, close to the heel of the dam, and the location of the seepage curtain also follow the guidelines usually adopted for Portuguese dams. The consideration of the rock wedge downstream of the dam is based on the existing conditions of the Pedrogão dam [42].

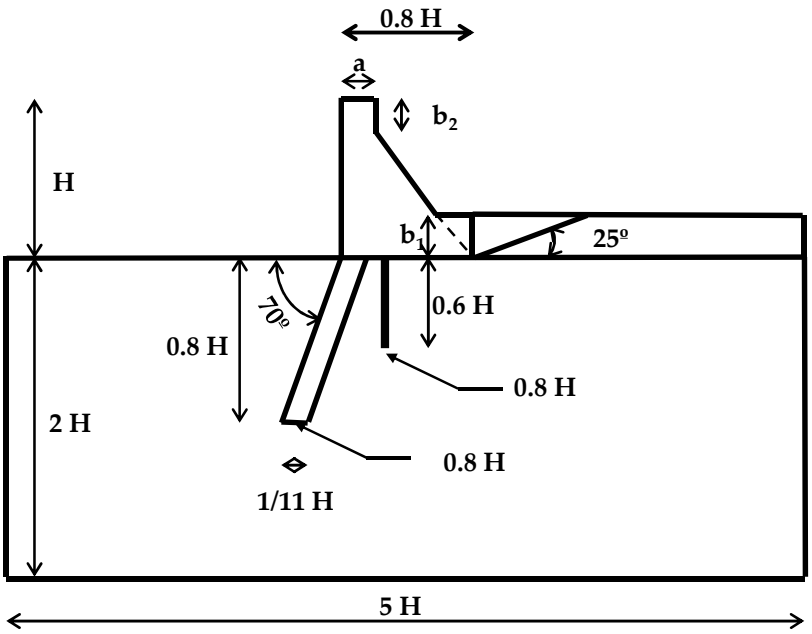

Figure 4. Adopted model geometry—usual dimensions in terms of the dam height (H).

Table 1. Geometry model parameters.

Dam Model	H (m)	a (m)	b1 (m)	b2 (m)
Dam 15	15	4.0	3.0	5.0
Dam 30	30	7.5	6.0	9.0
Dam 60	60	8.5	12.0	10.2

The foundation rock masses were represented with two families of discontinuities:

(i) One model, called "reg", was considered with the following:
   a. A family of continuous horizontal discontinuities with spacings of 2.5 m in the 15 m high dam models, 5.0 m in the 30 m high dam models, and 10.0 m in the 60 m high dam models;
   b. A family formed by vertical discontinuities with an average spacing of 2.5 m and a standard deviation of 1.0 m in the 15 m high dam models, an average spacing of 5.0 m and a standard deviation of 2.0 m in the 30 m high dam models, and an average spacing of 10.0 m and a standard deviation of 4.0 m in the 30 m high dam models;

(ii) Another model was considered, called "dip", with families of continuous orthogonal discontinuities that make angles of 15° and 105° with the horizontal.

In the latter case, the orientation and the fact that the families of discontinuities are continuous and flat favor the formation of failure mechanisms, with the formation of wedges that can slide under the dam.

To increase the complexity of the failure mode associated with the dam–foundation stability scenario (strength reduction or load amplification), it was considered that the foundation downstream from the dam is at a higher level, contributing to the dam stability.

An additional discontinuity was imposed downstream from the toe of the dam, creating a wedge that allowed sliding to occur even if elastic foundation behavior was assumed.

In the concrete dam, a set of horizontal continuous discontinuities were assumed. These discontinuities were located 3.0 m apart in the model with the dam 15 m in height (5 dam blocks), 2.0 m apart in the 30 m high dam model (15 blocks) and 4.0 m apart in the 60 m high dam model (15 blocks). The objective was not only to simulate dam lift joints but also to allow the mechanism failure to include the dam body.

Table 2 shows the numbers of mechanical and hydraulic elements used in the six dam–foundation models. The average edge lengths of the triangular elements were set as follows:

- A length of 0.5 m in the 15 m high concrete dam models (Dam 15-reg and Dam 15-dip);
- A length of 1.0 m in the 30 m high concrete dam (Dam 30-reg and Dam 30-dip);
- A length of 2.0 m in the 60 m high concrete dam (Dam 60-reg and Dam 60-dip).

Table 2. Hydromechanical discontinuum model summary.

Dam Height	Foundation Type	Mechanical Model				Hydraulic Model	
		Blocks	Nodes	FE Triangular Elements	FE Joint Elements	Hydraulic Nodes	Seepage Channels
15	reg	403	11,941	15,449	3588	3602	3317
	dip	431	11,922	15,045	3745	3760	3446
30	reg	416	11,933	15,364	3616	3631	3337
	dip	446	11,967	15,137	3735	3749	3440
60	reg	419	11,966	15,362	3652	3666	3367
	dip	467	11,948	14,991	3773	3787	3465

2.5. Hydromechanical Model Parameters

Both the dam concrete and rock mass blocks were assumed to follow elastic linear behavior, with the properties shown in Table 3, which match the experimental properties of the granite and concrete adopted in [24].

Table 3. Mechanical model elastic and strength properties—reference model.

(a) Plane FE elements			
Material	E **(GPa)**	v **(-)**	ρ **(kg/m^3)**
Dam concrete	30.3	0.24	2.4
Rock mass	64.4	0.20	2.7

(b) Joint FE elements							
Interface	k_n **(GPa/m)**	k_s **(GPa/m)**	σ_t **(MPa)**	C_{max} **(MPa)**	μ_c **(-)**	G_I **(Nm/m^2)**	G_{II} **(Nm/m^2)**
Concrete–Concrete	60.6	24.2	2.88	5.76	1.0	87.0	435.0
Concrete–Rock	128.8	51.5	1.37	2.74	1.0	24.7	123.3
Rock–Rock	128.8	51.5	0.0	0.0	-	-	-

Table 3b presents the adopted interface elastic and strength contact model parameters. The concrete–concrete and concrete–rock interfaces followed a bilinear softening model (see Section 2.1). Also presented are the rock–rock interface strength properties when a nonlinear foundation model was adopted, where zero tensile and cohesion stress and a friction coefficient of 1.0 were assumed. The normal and shear stiffness values should

be as high as required to ensure that the deformation occurs mainly within the blocks; but, to ensure numerical robustness, the maximum values need to be limited. The normal stiffness values were defined as if the joint had a fictitious thickness of 0.50 m, and a ratio of 0.4 was assumed between the normal and shear stiffnesses, which are within the usual values adopted for discrete media [42,44].

The tensile strength (σ_t) and the fracture energy (G_I) adopted for the concrete–concrete interface correspond to the experimental values obtained for concrete [24]. The tensile strength (σ_t) and the fracture energy in mode I (G_I) adopted for the concrete–rock interface correspond to the properties presented in [24] for specimen TPB 5-5, which correspond to the best-fit bilinear softening model that predicted an excellent agreement with the experimental results. The cohesive stress (C_{max}) and the fracture energy in mode II (G_{II}) were defined for both contact interfaces adopting the following relationships of $C_{max} = 2.0\,\sigma_t$ and $G_I = 5.0\,G_{II}$. The adopted values were within the range of values usually adopted for BL contact models representing concrete and rock material [40,43]. In [53,54], a factor of 1.75 was adopted for the cohesive stress and a factor of 2.0 was adopted for the fracture energy in mode II. A friction angle of 1.0 was also adopted for both interfaces, which is also within the usually adopted values.

The following hydraulic apertures were considered: a_0 = 0.1668 mm, $a_{res} = \frac{1}{3}\,a_0$ and $a_{max} = 5\,a_0$ [42]. It was assumed that the permeability of the dam–foundation interface was half of the foundation discontinuity permeability. In the grout curtain vicinity, a permeability 2.5 times lower than that adopted for the rock mass was considered. The dam construction joints were impervious.

The hydraulic parameters were within the range of the parameters adopted in [42], which have been shown to predict the observed hydraulic behavior of a Portuguese gravity dam. In [42,55], a grout curtain with a permeability 10.0 times lower than that of the rock mass was adopted, whereas a lower value of 2.5 was adopted in this work. Note that the grout curtain permeability has a noticeable influence on the quantity of water that flows through the foundation: a lower permeability value is associated with a lower water flow but has little influence on the pressure distribution, which is the main parameter that affected the stability studies that are presented here [55].

2.6. Hydromechanical Model Boundary Conditions and Analysis Sequence

Concerning the mechanical boundary conditions, the base of the model was fixed, and horizontal displacements perpendicular to the lateral boundaries were prevented. As for the hydraulic boundary conditions, zero permeability was assumed at the base and lateral boundaries of the model, and the drainage system was simulated by assigning water pressures along the drain axis equivalent to one-third of the hydraulic head upstream from the dam.

The models developed were used to assess the sliding safety of the dam–foundation system. The analysis was carried out in two phases: First, a hydromechanical calculation was carried out, considering the weight of the dam, assuming that the water table was at ground level and that the ratio between the horizontal and vertical effective stresses in situ was equal to 0.5. In the second phase, with the reservoir assumed to be at the dam crest level, the hydrostatic pressure was applied at the upstream face of the dam and at the base of the reservoir, assuming that all the discontinuities had linear elastic behavior. In this phase, a coupled hydromechanical analysis was carried out. In cases where the nonlinear behavior of the discontinuities was assumed, this was only considered after equilibrium had been reached, assuming linear elastic behavior.

Subsequently, for each gravity dam, an overtopping scenario was assessed by gradually increasing the reservoir water level using 1 m height increments.

Three different calculation hypotheses were considered:

- The uncoupled approach (UCP)—In the UCP approach, the hydraulic model pressures are kept constant during the process of increasing the water level above the dam crest. In this approach, the uplift pressures are not influenced by the subsequent changes in the mechanical apertures or by the water level rise that just affects the mechanical model;
- The coupled approach (CP)—In the CP approach, the water level rise above the dam crest influences both the mechanical model (hydrostatic pressure at the upstream face of the dam and upstream foundation surface) and the hydraulic model (applied hydraulic-imposed pressure at the reservoir bottom). In this approach, a coupled calculation is performed for each water level, so the mechanical aperture variations affect the hydraulic model and the pressure variations in the hydraulic model affect the mechanical apertures. Seepage occurs in all interfaces independently of their damage (the corresponding water pressures are installed from the beginning of the simulation on all interfaces);
- The coupled approach taking into account fracture propagation at the dam–foundation interface (CP-FP)—The CP-FP approach is similar to the CP approach, with one exception: seepage is only allowed to occur at the dam–foundation interface after cracking occurs, making it possible to model the fracture propagation along the dam–foundation interface due to a hypothetical dam overtopping scenario. In all other interfaces, seepage occurs independently of their damage, as adopted in the CP approach.

For each calculation hypothesis, two different foundation behaviors were assessed: an elastic model (E) and a brittle model (B), following the properties presented in Table 3 for rock–rock contacts. For the reference model properties, a stability analysis based on the strength reduction approach, usually adopted in dam design [36,56,57], was also carried out. In this analysis, zero tensile and cohesion stresses were adopted at the concrete–rock interface, and the frictional term of the corresponding joint elements was gradually reduced up to failure.

3. Results and Discussion

3.1. Pressure Distribution Before Load Amplification/Strength Reduction

Figure 5 shows the piezometric head pseudo-equipotential contours for the model 60-reg for both elastic and brittle foundation behavior for the case where seepage was considered along the dam–foundation interface for a water height corresponding to the dam crest level (the UCP and CP approaches) and for the case where seepage along the dam–foundation interface was only allowed after damage initiation at each joint element (the CP-FP approach). The term pseudo-equipotential is adopted because of the discrete nature of the flow that occurs along the rock mass discontinuities.

As shown, in the vicinity of the dam foundation and both upstream and downstream from the dam, the hydraulic head has some differences. Compared with the UCP and CP approaches, with the FP-CP approach, the hydraulic head is slightly lower in the vicinity of the dam–foundation interface and slightly more pronounced at higher depths in the upstream area. The effect of the adopted foundation model on the hydraulic head distribution is also visible: with brittle foundation behavior, higher hydraulic heads were recorded at higher depths and in closer proximity to the dam heel. The effect of the drainage system on the hydraulic head is visible in all the calculations.

Figure 6 shows the distribution of the water pressures along the base of the dam obtained for the two seepage assumptions assuming a brittle foundation. As shown, in the CP-FP approach, at the beginning of the load amplification procedure, there was no

damage at the dam–foundation interface joint elements (zero pressure), whereas in the scenario where seepage was allowed from the beginning of the calculation (the UCP and CP approaches), the predicted pressure distribution is closer to a bi-linear uplift distribution, which is usually assumed in stability design.

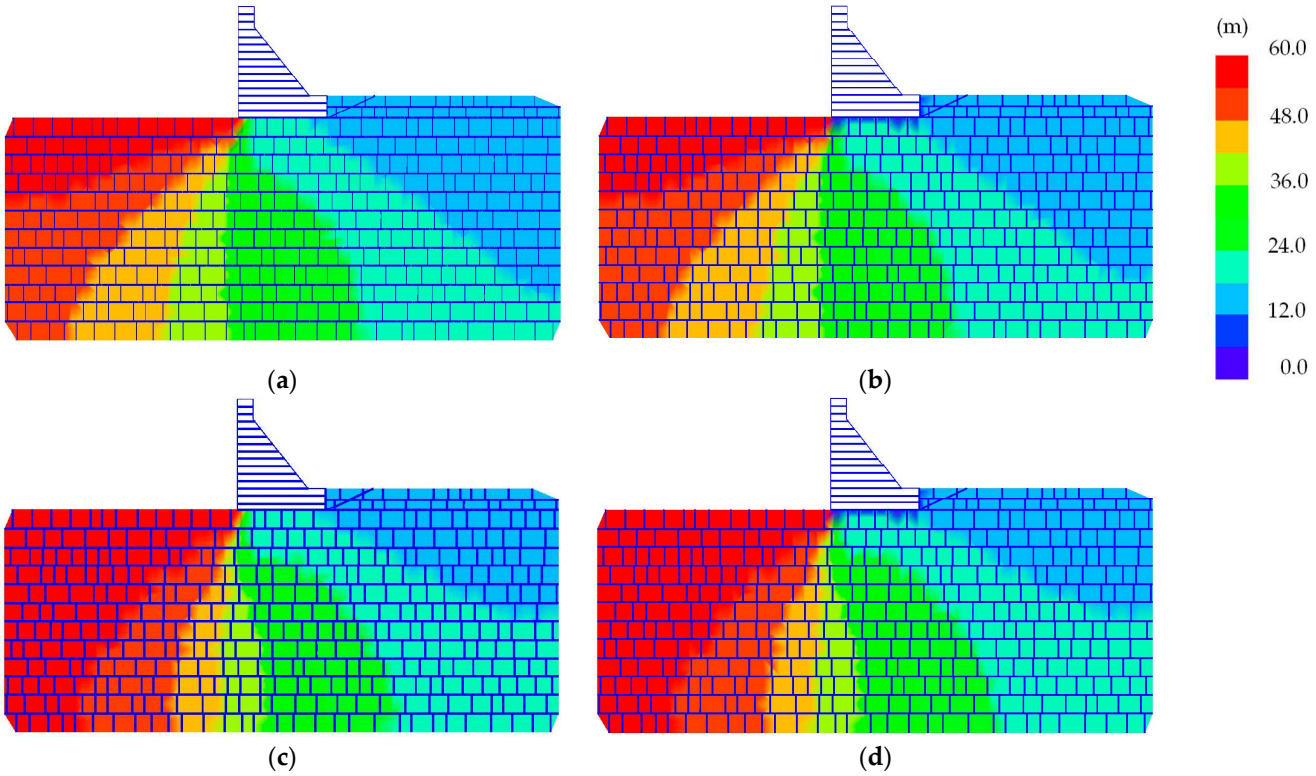

Figure 5. Piezometric head pseudo-equipotential contours: model 60-reg. (**a**) UCP and CP (elastic foundation); (**b**) CP-FP (brittle foundation); (**c**) UCP and CP (brittle foundation); and (**d**) CP-FP (brittle foundation).

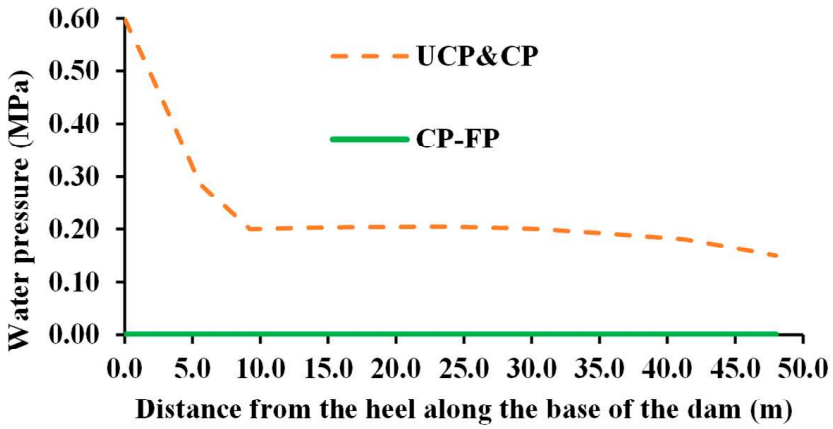

Figure 6. Water pressure along the base of the dam: model 60-reg (brittle foundation).

3.2. Strength Reduction Method—Project Design

For comparison reasons, the stability analysis was initially carried out using the resistance reduction method typically used in dam design [27,30,58]. This analysis was carried out using the discontinuous models developed, which take hydromechanical interaction into account. An initial friction angle of 45° was assumed for the concrete–rock interface. The JEs were assumed to follow brittle Mohr–Coulomb behavior. The friction coefficient of the rock–foundation discontinuity was gradually reduced until failure occurred.

As mentioned, two different foundation behaviors were assessed: an elastic model (E) and a brittle model (B), using the properties presented in Table 3, except for the concrete–rock interface, which, as mentioned, followed a pure-friction model, and the rock–rock interface of the rock–foundation wedge downstream from the dam, which also followed a pure-friction model with a constant friction coefficient of 1.0.

Table 4 presents the strength reduction stability safety factors for the different dam models, foundation behaviors and drainage conditions. As shown, the dam foundation does not have a meaningful influence on the predicted safety factor. The dam height influence is also not that significant; the safety factor has a slight decrease for the 60 m high dam. Also, as expected, when the drains are for some reason not working, the predicted stability safety factors through a strength reduction factor decrease (a 13% to 18% reduction) and follow the same trends that are described for the working drain case.

Table 4. Strength reduction safety factors—strength reduction—reference model.

(a) Drainage system working properly—with downstream wedge						
Foundation Behavior	**Dam Model**					
	15-reg	**15-dip**	**30-reg**	**30-dip**	**60-reg**	**60-dip**
E	2.20	2.20	2.20	2.20	2.10	2.10
B	2.20	2.20	2.20	2.20	2.10	2.10
(b) Drainage system clogged—with downstream wedge						
Foundation Behavior	**Dam Model**					
	15-reg	**15-dip**	**30-reg**	**30-dip**	**60-reg**	**60-dip**
E	1.90	1.90	1.90	1.80	1.80	1.80
B	1.90	1.80	1.80	1.80	1.80	1.80
(c) Drainage system working properly—without downstream wedge						
Foundation Behavior	**Dam Model**					
	15-reg	**15-dip**	**30-reg**	**30-dip**	**60-reg**	**60-dip**
E	1.70	1.70	1.70	1.70	1.50	1.50
B	1.70	1.70	1.70	1.70	1.50	1.50

For comparison purposes, Table 4c also shows the strength reduction stability factors assuming that the drainage system is working properly and neglecting the contribution of the foundation rock above the dam foundation level. As shown, the safety factors follow the same trends as those when the downstream foundation contribution is considered, but as expected, without the downstream foundation contribution, the predicted safety factors are noticeably lower.

Figure 7 shows the predicted failure modes for the 60 m high dam for both foundation geometries, assuming that the drainage system is working properly. As shown, the failure modes in the four different analyses correspond to the expected shear sliding along the dam–foundation interface, with the corresponding downstream wedge also sliding. Similar failure modes were obtained with the dam models 15 m and 30 m high.

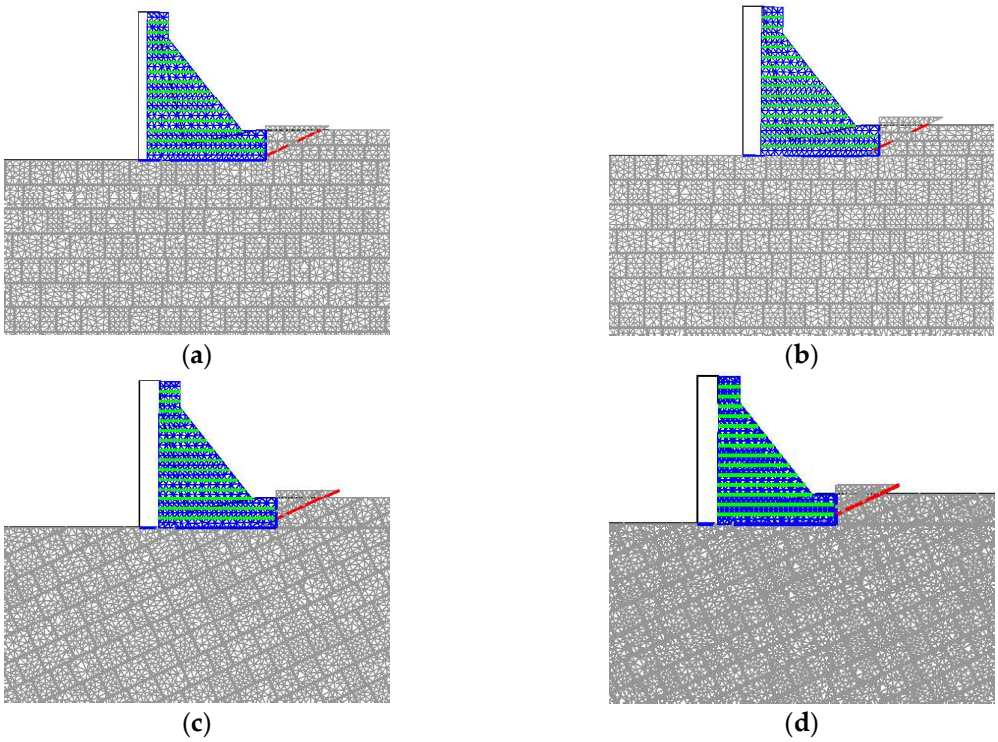

Figure 7. Failure modes associated with the Dam 60-reg and Dam 60-dip hydromechanical discontinuum models of the dam–foundation system (200× amplification factor). (**a**) Dam 60-reg dam–foundation elastic behavior (E); (**b**) Dam 60-reg dam–foundation nonlinear behavior (B); (**c**) Dam 60-dip dam–foundation elastic behavior (E); and (**d**) Dam 60-dip dam–foundation nonlinear behavior (B).

3.3. Overtopping Scenario—Load Amplifcation

3.3.1. Reference Model Parameters

The stability analysis of the dam–foundation systems was also carried out by amplifying the hydrostatic loads by gradually increasing the reservoir water level using 1 m high increments to simulate an overtopping scenario. Like in the previous example, for each dam height and dam geometry, two different foundation behaviors were assessed: an elastic model (E) and a brittle model (B), using the properties presented in Table 3. For each case, three different calculation hypotheses were considered: the uncoupled approach (UCP), the coupled approach (CP) and the coupled approach considering fracture propagation along the dam–foundation interface (CP-FP).

In a preliminary assessment, the UCP approach is expected to be the most conservative approach with higher associated safety factors, as only the mechanical pressures are increased, and the water pressures in the hydraulic model are kept constant throughout the calculation. The CP-FP approach is expected to be the least conservative approach because in the vicinity of the dam–foundation, seepage is only allowed to occur when the joint elements are found to be cracked (see Section 3.1).

Table 5 shows the numerically predicted shear sliding safety factors for an overtopping scenario obtained for the six adopted dam–foundation systems, assuming that the drainage is operable (Table 5a) and the drainage system is clogged (Table 5b). Table 5a shows the following:

- For an elastic foundation model (E), the UCP always predicts a higher safety factor (≈20% higher) than those predicted with the CP and CP-FP approaches. For brittle behavior, the UCP safety factors are still higher than those predicted with the CP and

CP-FP approaches but are more scattered and lower than those predicted with an elastic foundation (≈6.5 to 17% higher);

- For an elastic foundation, the CP- and the CP-FP-associated shear sliding safety factors are similar, except for the model 30-dip, where, contrary to the expected, the CP approach predicted a safety factor 3% higher than that predicted with the CP-FP approach. With the brittle foundation, the sliding safety factors of the CP and CP-FP approaches are similar, except for the model 30-reg and model 60-dip, where the CP-FP safety factors are slightly higher than those predicted with the CP-FP approach (≈1.5 to 11.6% higher);
- For a brittle foundation (B) and for the 15 m high dam, the predicted safety factors are higher than those predicted with elastic behavior, whereas for the 30 m high dam and 60 m high dam, the predicted safety factors are lower than those predicted with the elastic model, with the exception of the safety factors predicted with the CP-FP approach for the models 30-reg, 30-dip and 60-dip.

Table 5. Overtopping scenario—safety factors—reference model.

(a) Drainage system working properly							
Foundation Behavior	**Approach**	**Dam Model**					
		15-reg	**15-dip**	**30-reg**	**30-dip**	**60-reg**	**60-dip**
E	UCP	3.67	3.67	3.27	3.33	3.00	3.00
	CP	2.87	2.87	2.60	2.67	2.43	2.40
	CP-FP	2.87	2.87	2.60	2.60	2.43	2.40
B	UCP	3.93	3.80	3.07	3.07	2.77	2.73
	CP	3.40	3.00	2.53	2.60	2.30	2.40
	CP-FP	3.40	3.00	2.87	2.60	2.30	2.43
(b) Drainage system clogged [1]							
Foundation Behavior	**Approach**	**Dam Model**					
		15-reg	**15-dip**	**30-reg**	**30-dip**	**60-reg**	**60-dip**
E	UCP	3.00 (−18.2)	3.00 (−18.2)	2.73 (−16.3)	2.73 (−18.0)	2.43 (−18.9)	2.43 (−18.9)
	CP	2.47 (−14.0)	2.33 (−18.6)	1.93 (−25.6)	1.93 (−27.5)	1.73 (−28.8)	1.73 (−27.8)
	CP-FP	2.87 (0.0)	2.47 (−14.0)	1.87 (−28.2)	1.80 (−30.8)	1.73 (−28.8)	1.73 (−27.8)
B	UCP	3.53 (−10.2)	3.13 (−17.5)	2.73 (−10.9)	2.60 (−15.2)	2.20 (−20.5)	2.30 (−15.9)
	CP	2.87 (−15.7)	2.20 (−26.7)	2.27 (−10.5)	2.00 (−23.1)	1.80 (−21.7)	1.83 (−23.6)
	CP-FP	2.73 (−19.6)	2.33 (−22.2)	2.27 (−20.9)	2.00 (−23.1)	1.97 (−14.5)	1.83 (−24.7)

[1] The differences to the safety factors presented in Table 5a, in percentages, are shown in brackets.

Interestingly, for the reference contact strength parameters (Table 3), considering the fracture propagation (CP-FP) at the dam–foundation interface did not significantly influence the predicted safety factors when compared with the CP approach. It is also interesting to note that an elastic foundation assumption does not always lead, when compared with the safety factor obtained with brittle foundation behavior, to a lower associated safety factor.

Table 5b shows the safety factors obtained assuming that the drainage system is clogged. Also shown, in brackets, are the differences, in percentages, to the safety factors obtained assuming that the drainage system is working properly. Table 5b shows that for the clogged drainage system scenario, the safety factors predicted with the CP and CP-FP approaches have more noticeable differences than those obtained assuming the working drainage system scenario, showing that the seepage along the dam–foundation interface is more relevant under the clogged drainage system hypothesis. For the models 15-reg

and 15-dip with an elastic foundation and for the models 15-dip and 60-reg with a brittle foundation, the CF-FP-predicted safety factors are slightly higher than those predicted with the CP approach. In contrast, for the models 30-reg and 30-dip under an elastic foundation assumption and for the model 15-reg under a nonlinear foundation, the CP-FP-associated safety values are slightly higher than those predicted with the CP approach.

Figures 8–10 show the horizontal crest displacement during the simulation of a gradual increase in the reservoir level, assuming that the drainage system is working properly, for the 15 m high, 30 m high and 60 m high dams, respectively. As shown, for all dam heights and foundation behaviors, the UCP approach led to the highest stable water heights. As expected, the UCP response was similar to the CP and CP-FP responses until a certain water level was reached. Under the CP and CP-FP approaches, for a given water level value, the associated water pressures start to be an important loading factor that contributes to the rotation of the dam, which is more noticeable under brittle behavior. It is also shown that the response under an elastic foundation assumption (E) has some differences when compared with the predicted response under brittle behavior (B). Under brittle foundation behavior, the influence of the foundation geometry is also more evident.

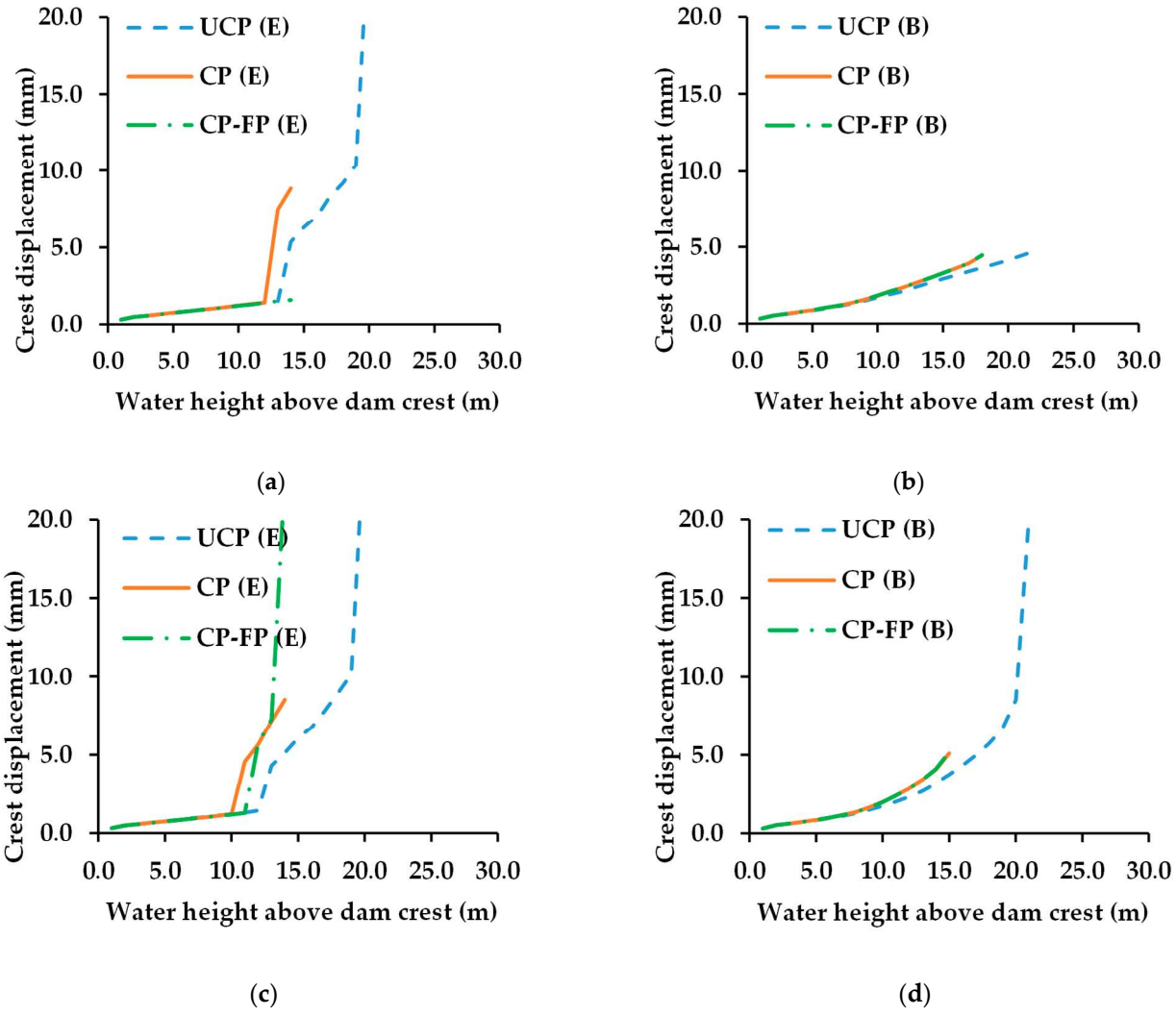

Figure 8. Horizontal crest displacement during the overtopping scenario assessment for models 15-reg and 15-dip. (**a**) Dam 15-reg dam–foundation elastic behavior (E); (**b**) Dam 15-reg dam–foundation nonlinear behavior (B); (**c**) Dam 15-dip dam–foundation elastic behavior (E); and (**d**) Dam 15-dip dam–foundation nonlinear behavior (B).

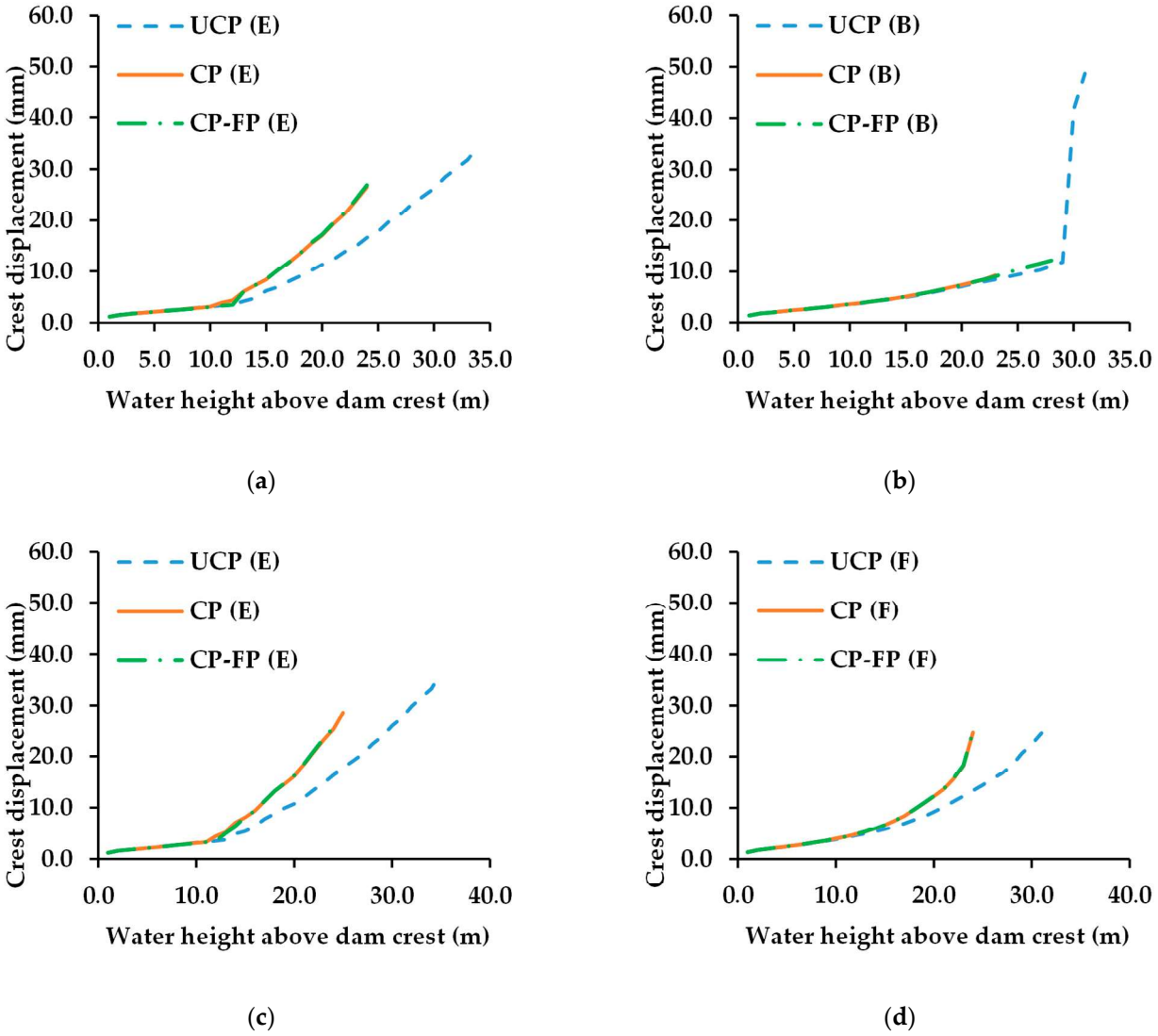

Figure 9. Horizontal crest displacement during the overtopping scenario assessment for models 30-reg and 30-dip. (**a**) Dam 30-reg dam–foundation elastic behavior (E); (**b**) Dam 30-reg dam–foundation nonlinear behavior (B); (**c**) Dam 30-dip dam–foundation elastic behavior (E); and (**d**) Dam 30-dip dam–foundation nonlinear behavior (B).

Under drained conditions and the CP-FP approach, the following was observed:

- Fracture propagation at the dam–foundation interface only occurred at the maximum water height or closer to the maximum value, and a fully damaged interface developed (dam 15-reg (E), dam15-dip (E), dam 15-reg (B), dam30-reg (B));
- Fracture propagation at the dam–foundation interface only occurred at the maximum water height or closer to the maximum value, but only partial damage occurred at the dam–foundation interface (dam 15-dip (B), dam30-dip (B));
- Fracture propagation at the dam–foundation interface occurred before the maximum water height was reached, but at failure, the entire dam–foundation were found to be cracked (dam 30-reg (E), dam 30-dip (E));
- Fracture propagation at the dam–foundation interface occurred before the maximum water height was reached for a lower height under elastic foundation behavior, but the dam–foundation were found to be partially cracked (80% or less) (dam 60-reg (E), dam 60-dip (E), dam 60-reg (B), dam 60-dip (B));
- Localized damage (less than 2%) was found to occur in concrete in all the dam models with dam heights higher than 15 m.

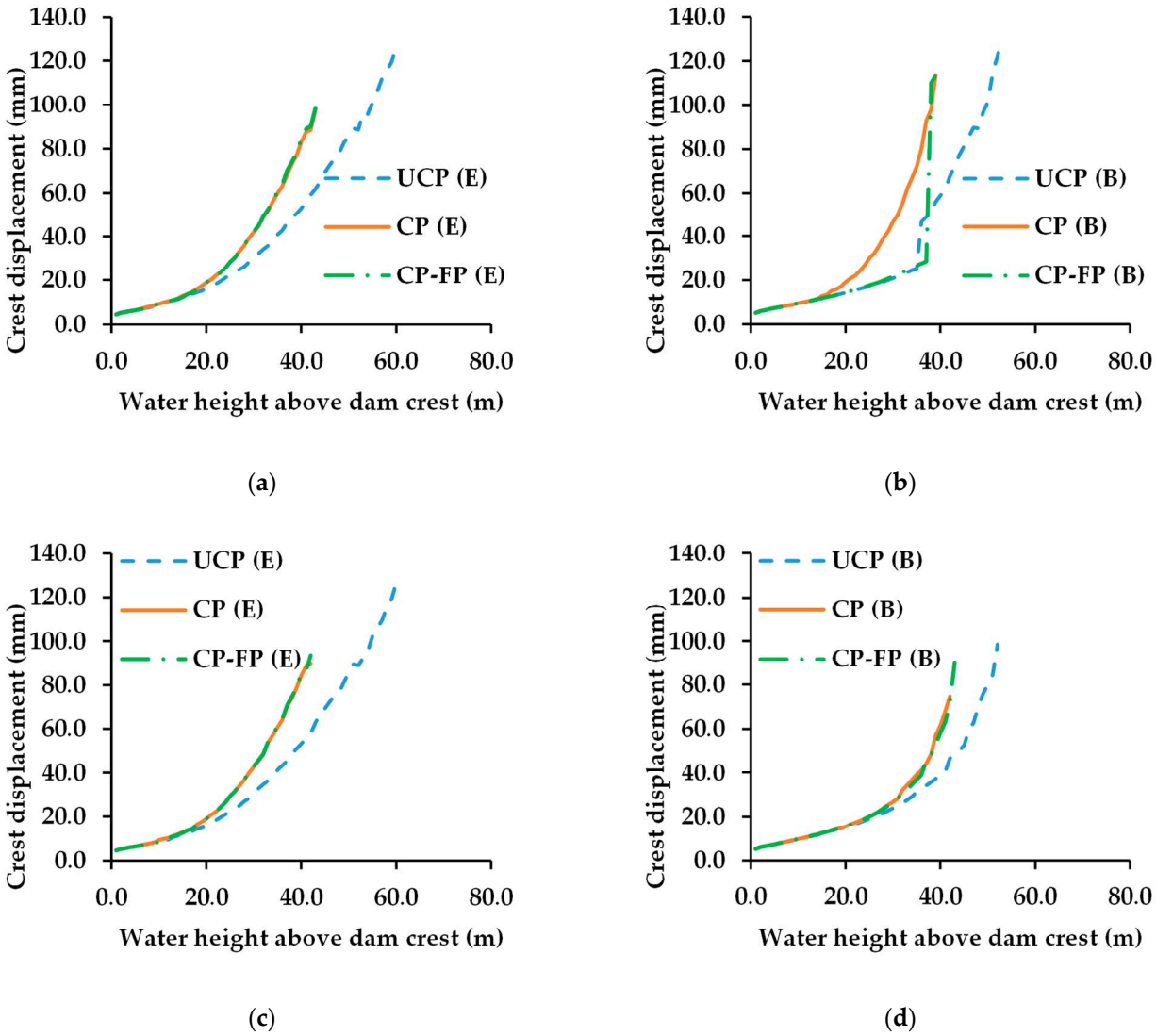

Figure 10. Horizontal crest displacement during the overtopping scenario assessment for models 60-reg and 60-dip. (**a**) Dam 60-reg dam–foundation elastic behavior (E); (**b**) Dam 60-reg dam–foundation nonlinear behavior (B); (**c**) Dam 60-dip dam–foundation elastic behavior (E); and (**d**) Dam 60-dip dam–foundation nonlinear behavior (B).

Under clogged conditions and the CP-FP approach, when compared with the results obtained with an operational drainage system, a higher number of models only had fracture at the maximum water height, and localized fracture in concrete occurred in less models, overall:

- Fracture propagation at the dam–foundation interface only occurred at the maximum water height or closer to the maximum value, and a fully damaged interface developed (dam 15-reg (E), dam15-dip (E), dam 15-reg (B), dam 15-dip (B), dam30-reg (B), dam30-dip (B)), dam 60-reg (B);
- Fracture propagation at the dam–foundation interface occurred before the maximum water height was reached, but at failure, the entire dam–foundation were found to be cracked (dam 30-reg (E), dam 30-dip (E));
- Fracture propagation at the dam–foundation interface occurred before the maximum water height was reached for a lower height under elastic foundation behavior, but the dam–foundation were found to be partially cracked (80% or less) (dam 60-reg (E), dam 60-dip (E), dam 60-dip (B));

- Localized damage (less than 2%) was found to occur in concrete in all the models at failure under drained conditions for a dam height higher than 15 m, except for models dam30-reg (E) and dam30-dip (E).

Figure 11 shows the predicted failure modes for the 15 m high dam for both foundation geometries for the working drainage system scenario for the CP approach and for both foundation behaviors. Note that the failure modes with the UCP and CP-FP approaches are very similar to that obtained with the CP approach for all the studied scenarios. For the regular dam geometry (reg), it is shown that all the different seepage approaches predicted similar complex failure modes: the sliding of the dam is accompanied by rotation at the downstream foot. For the irregular foundation geometry, there are some differences between the failure mode predicted for an elastic foundation and that predicted for a brittle foundation, whereas with an elastic foundation, the failure mode is similar to that predicted for a regular foundation, and for a brittle foundation, the failure mode is also due to the rotation of the dam in the downstream toe, but it also includes the foundation blocks in the vicinity of the dam–foundation interface.

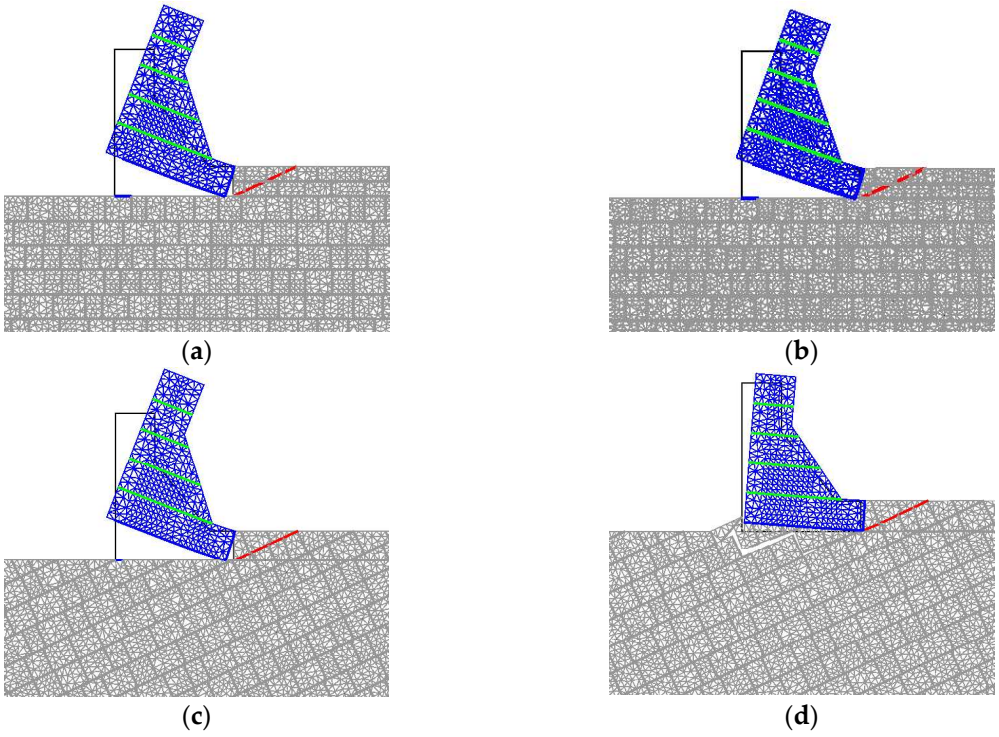

Figure 11. Failure modes associated with the Dam 15-reg and Dam 15-dip hydromechanical discontinuum models of the dam–foundation system (100× amplification factor). (**a**) Dam 15-reg CP (E); (**b**) Dam 15-reg CP (B); (**c**) Dam 15-dip CP (E); (**d**) Dam 15-dip CP (B).

Figures 12 and 13 show the predicted failure modes for the 60 m high dam for the regular foundation and irregular foundation, respectively, for a working drainage system scenario for the UCP and CP approaches for both assessed foundation behaviors. Note that the failure mode predicted with the CP-FP approach is very similar to that obtained with the CP approach for all the studied scenarios. For the regular dam foundation (Figure 12), it is shown that all the different seepage approaches predicted complex failure modes similar to the one predicted for the 15 high dam, with the exception that for the 60 m high dam, a larger support base at the downstream toe is identified. The only exception is the failure mode predicted with the UCP approach for an elastic foundation, which also included failure in the dam body at a mid-height lift joint.

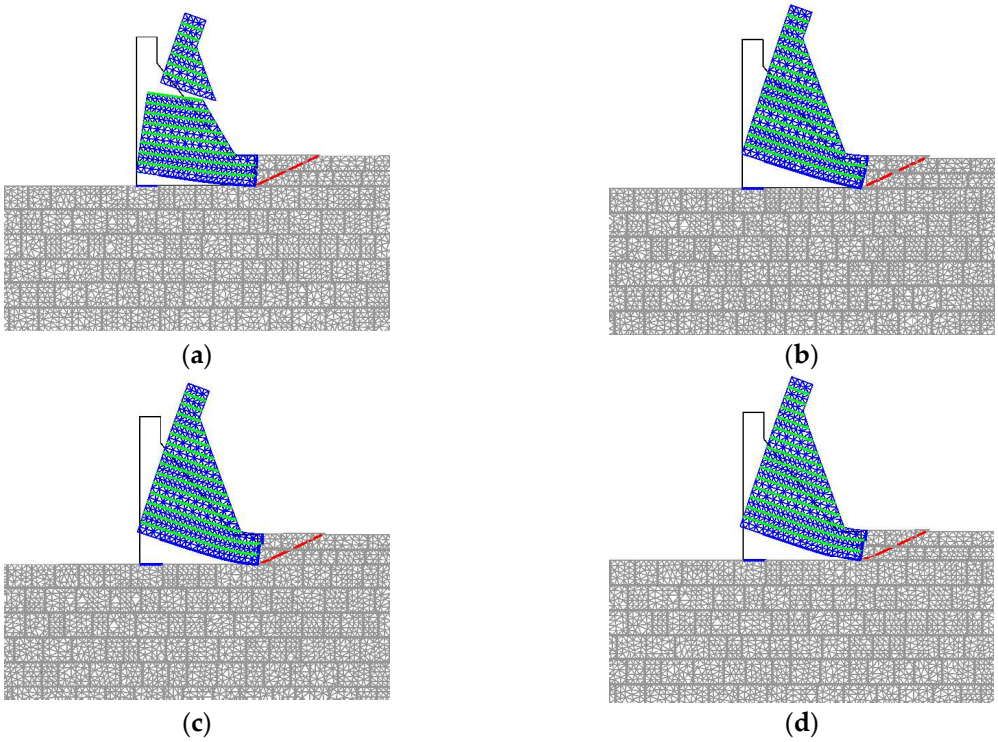

Figure 12. Failure modes associated with the Dam 60-reg hydromechanical discontinuum model of the dam–foundation system (100× amplification factor). (**a**) Dam 60-reg UCP (E); (**b**) Dam 60-reg UCP (B); (**c**) Dam 60-reg CP (E); (**d**) Dam 60-reg CP (B).

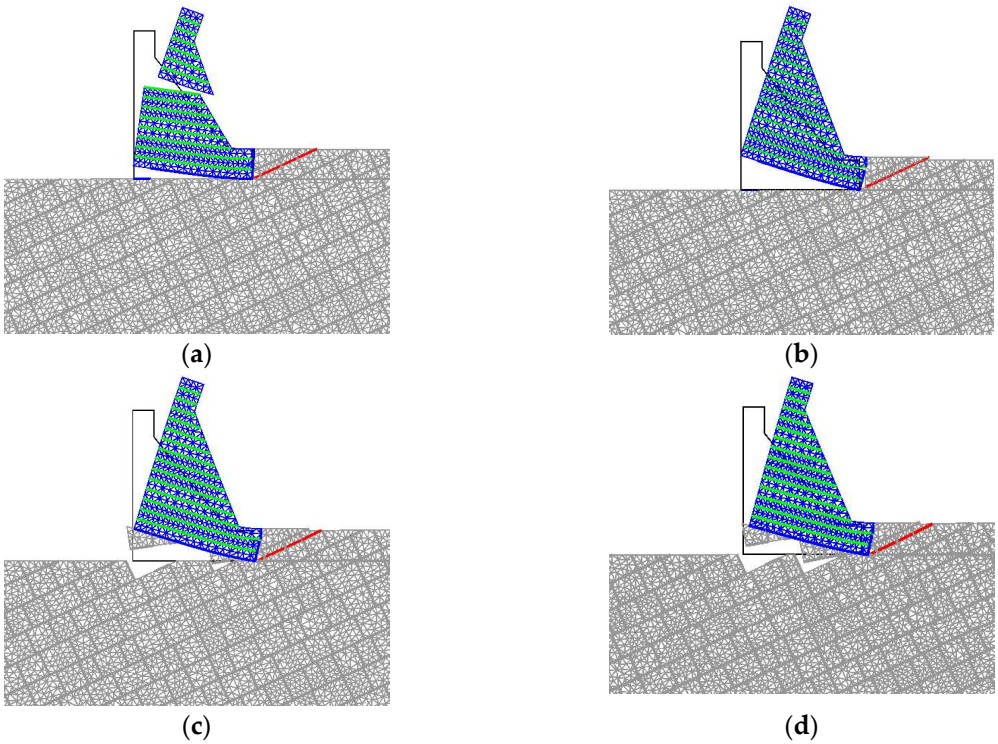

Figure 13. Failure modes associated with the Dam 60-dip hydromechanical discontinuum model of the dam–foundation system of (100× amplification factor). (**a**) Dam 60-dip UCP (E); (**b**) Dam 60-dip UCP (B); (**c**) Dam 60-dip CP (E); (**d**) Dam 60-dip CP (B).

For the irregular dam foundation (Figure 14) for elastic foundation behavior, the failure modes are similar to the failure modes predicted with a regular foundation. There are some differences between the failure mode predicted for an elastic foundation and the failure

mode predicted for a brittle foundation: for a brittle foundation, the failure mode also includes the foundation blocks in the vicinity of the dam–foundation interface.

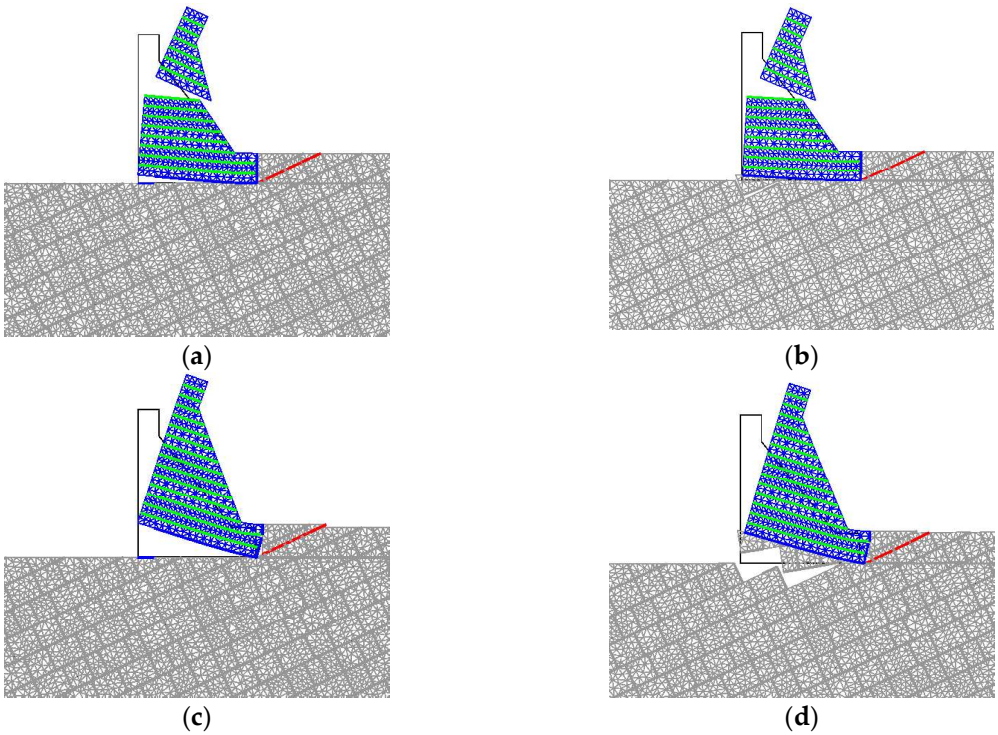

Figure 14. Failure modes associated with the Dam 60-dip hydromechanical discontinuum model of the dam–foundation system (100× amplification factor). (**a**) UCP (E); (**b**) UCP (B); (**c**) CP (E); (**d**) CP (B).

3.3.2. Assessment of the Concrete–Rock Interface Ductility

To assess the influence of the concrete–rock interface ductility on the overall response for an overtopping scenario, two additional stability studies were carried out. In one study, a fracture energy in mode I ten times higher than the value presented in Table 3 was adopted, and in a subsequent study, a brittle model was adopted for the concrete–rock interface. It is important to note that the definition of the fracture energy in mode I requires a more complex experimental program when compared with the case where only the determination of the tensile strength is required [24].

Table 6 shows the numerically predicted shear sliding safety factors for an overtopping scenario obtained for the six adopted dam–foundation systems for a 10-fold increase in the fracture energy in mode I (Table 6a) and for a brittle concrete–rock interface model (Table 6b). Overall, an increase in the concrete–rock interface ductility led to an increase in the predicted safety factors, with few exceptions, namely, for the 15 m high dam and brittle foundation behavior, for which similar safety factors were predicted.

As shown in Table 6a, an increase in the concrete–rock interface ductility in mode I led to a more pronounced increase in the safety factors predicted with the CP-FP approach, especially for elastic foundation behavior and lower dam heights. With a higher fracture energy, the fracture propagation along the dam–foundation interface was more restrained when compared with the brittle contact model or bilinear contact model with lower fracture energy in mode I.

For the 15 m high dam and an elastic foundation, an increase of approximately 25% occurred in the safety factor predicted with the CP-FP approach, whereas for the dam 60 m high, the increase in the safety factor was in the order of 1% of the value obtained for the reference parameters. For brittle foundation behavior, the predicted increase in the

safety factors when adopting a more ductile law was less pronounced when compared with the increase obtained for an elastic foundation. For a higher concrete–rock ductility, the CP-FP approach was, for almost all the assessed scenarios, the least conservative approach, showing the relevance of the fracture energy to restraining the fracture propagation along the dam–foundation interface.

Table 6. Overtopping scenario—safety factors—fracture energy in mode I assessment.

(a) Higher fracture energy in mode I ($G_I = 10 \times G_I$ of Table 3) [1]

Foundation Behavior	Approach	Dam Model					
		15-reg	15-dip	30-reg	30-dip	60-reg	60-dip
E	UCP	4.07 (10.9)	4.07 (10.9)	3.40 (4.1)	3.47 (4.0)	3.00 (0.0)	3.00 (0.0)
	CP	3.27 (14.0)	3.27 (14.0)	2.67 (2.6)	2.73 (2.5)	2.47 (1.4)	2.43 (1.4)
	CP-FP	3.93 (37.2)	3.80 (32.6)	2.67 (2.6)	2.73 (5.1)	2.47 (1.4)	2.47 (2.8)
B	UCP	4.60 (16.9)	3.80 (0.0)	3.13 (2.2)	3.27 (6.5)	2.77 (0.0)	2.93 (7.3)
	CP	3.93 (15.7)	3.00 (0.0)	2.73 (7.9)	2.73 (5.1)	2.30 (0.0)	2.47 (2.8)
	CP-FP	3.93 (15.7)	3.00 (0.0)	3.13 (9.3)	2.73 (5.1)	2.47 (7.2)	2.53 (4.1)

(b) Brittle model [1]

Foundation Behavior	Approach	Dam Model					
		15-reg	15-dip	30-reg	30-dip	60-reg	60-dip
E	UCP	3.67 (0.0)	3.67 (0.0)	3.27 (0.0)	3.33 (0.0)	3.00 (0.0)	3.00 (0.0)
	CP	2.87 (0.0)	2.87 (0.0)	2.60 (0.0)	2.67 (0.0)	2.43 (0.0)	2.43 (1.4)
	CP-FP	2.73 (−4.7)	2.87 (0.0)	2.60 (0.0)	2.60 (0.0)	2.43 (0.0)	2.40 (0.0)
B	UCP	3.93 (0.0)	3.80 (0.0)	3.07 (0.0)	3.13 (2.2)	2.80 (1.2)	2.87 (4.9)
	CP	3.40 (0.0)	3.00 (0.0)	2.53 (0.0)	2.60 (0.0)	2.30 (0.0)	2.47 (2.8)
	CP-FP	3.40 (0.0)	3.00 (0.0)	2.87 (0.0)	2.60 (0.0)	2.30 (0.0)	2.47 (1.4)

[1] The differences to the safety factors presented in Table 5a, in percentages, are shown in brackets.

For brittle concrete–rock interface behavior (Table 6b), the predicted safety factors are in the order of the safety factors predicted with the reference model parameters, which indicates that the mode I fracture energy value of 24.7 Nm/m^2 obtained in the experimental program [24] is a very low value. Note that, for low fracture energy values, it is not mandatory to adopt bilinear softening, as similar results are obtained with a brittle model.

3.3.3. Assessment of the Concrete–Rock Interface Strength

To assess the influence of the concrete–rock interface strength on the overall response for an overtopping scenario, two additional hypotheses were considered. In one study, the strength properties adopted for the concrete–concrete material were also adopted for the concrete–rock interface (Cs) (Table 3), and additionally, for both the concrete–concrete and concrete–rock, the strength properties defined in Table 7 were considered (Cc). The values presented in Table 7 are within the range of dam concrete properties [22,30] and, when compared with the properties presented in Table 3 for the concrete–rock interface, have a tensile strength in the order of the value adopted for the concrete–rock interface and a significantly higher fracture energy in mode I.

Table 7. Mechanical model strength properties in recent studies for dam concrete (Cc).

Interface	σ_t (MPa)	C_{max} (MPa)	μ_c (-)	G_I (Nm/m^2)	G_{II} (Nm/m^2)
Concrete–Concrete and Concrete–Rock	2.90	8.0	1.0	250.0	2500.0

Table 8 presents the numerically predicted shear sliding safety factors for an overtopping scenario obtained for the six adopted dam–foundation systems, the concrete–rock strength scenario (Cs) (Table 8a) and the concrete–rock and concrete–concrete strength scenario (Cc) (Table 8b). The results show that an increase in the concrete–rock interface strength led to an increase in the predicted safety factors for all the dam heights and seepage modeling approaches. With the contact properties in Table 7 (Cc), which have a significantly higher fracture energy in mode I, the increase in the predicted safety factors is even more noticeable. Interestingly, the predicted increase is more noticeable for an elastic foundation assumption and for lower dam heights.

Table 8. Overtopping scenario—safety factors—concrete–rock strength assessment.

(a) Concrete–rock with concrete–concrete with properties in Table 3 (Cs) [1]

Foundation Behavior	Approach	Dam Model					
		15-reg	**15-dip**	**30-reg**	**30-dip**	**60-reg**	**60-dip**
E	UCP	4.73 (29.1)	4.47 (21.8)	3.67 (12.2)	3.67 (10.0)	3.00 (0.0)	3.00 (0.0)
	CP	4.33 (51.2)	3.93 (37.2)	2.87 (10.3)	2.87 (7.5)	2.50 (2.7)	2.50 (4.2)
	CP-FP	4.47 (55.8)	4.20 (46.5)	2.80 (7.7)	2.87 (10.3)	2.50 (2.7)	2.47 (2.8)
B	UCP	5.80 (47.5)	3.80 (0.0)	3.87 (26.1)	3.40 (10.9)	2.87 (3.6)	3.03 (11.0)
	CP	4.73 (39.2)	3.13 (4.4)	3.40 (34.2)	2.73 (5.1)	2.47 (7.2)	2.57 (6.9)
	CP-FP	4.73 (39.2)	3.00 (0.0)	3.67 (27.9)	2.73 (5.1)	2.73 (18.8)	2.57 (5.5)

(b) Concrete–rock and concrete–concrete with properties in Table 7 (Cc) [1]

Foundation Behavior	Approach	Dam Model					
		15-reg	**15-dip**	**30-reg**	**30-dip**	**60-reg**	**60-dip**
E	UCP	5.00 (36.4)	5.00 (36.4)	3.67 (12.2)	3.73 (12.0)	3.03 (1.1)	3.00 (0.0)
	CP	4.60 (60.5)	4.47 (55.8)	2.87 (10.3)	2.93 (10.0)	2.53 (4.1)	2.50 (4.2)
	CP-FP	5.27 (83.7)	5.00 (74.4)	3.00 (15.4)	3.07 (17.9)	2.53 (4.1)	2.50 (4.2)
B	UCP	6.20 (57.6)	3.93 (3.5)	3.87 (26.1)	3.40 (10.9)	2.87 (3.6)	2.93 (7.3)
	CP	5.00 (47.1)	3.13 (4.4)	3.47 (36.8)	2.87 (10.3)	2.47 (7.2)	2.57 (6.9)
	CP-FP	5.00 (47.1)	3.13 (4.4)	3.93 (37.2)	2.87 (10.3)	2.80 (21.7)	2.57 (5.5)

[1] The differences to the safety factors presented in Table 5a, in percentages, are shown in brackets.

As shown in Table 8b for the contact properties defined in Table 7 (Cc), the safety factors predicted with the CP-FP approach, especially for elastic foundation behavior and lower dam heights, were always higher than the values predicted with the CP approach. As in the previous example, a higher fracture energy restrains fracture propagation along the dam–foundation interface, and the scenario wherein seepage was allowed after cracking occurred led to the expected slightly higher safety factors. Interestingly, under brittle foundation behavior and a dip geometry, the increase is more marginal, even for the higher-strength contact properties (Cc).

Figure 14 shows the predicted failure modes for the UCP and CP approaches for elastic foundation behavior and brittle foundation behavior for the 60 high dam and for an irregular dam foundation. The failure modes predicted with the CP-FP approach are similar to those predicted with the CP approach, where seepage occurred from the onset of the safety factor calculation. As shown, for a brittle foundation, the failure mode under the CP hypothesis was a coupled failure mode that also included the foundation in the vicinity of the concrete–rock interface. This complex failure mode may explain why the increase in the safety factor is not as noticeable as that under an elastic foundation or a regular foundation geometry; this occurred for the other dam heights as well (Table 8). Also, as shown in Figure 13b, contrary to the failure mode predicted with the reference parameters,

for the Cc concrete–rock parameters, the associated failure mode under a coupled approach was associated with failure within the concrete lift joint.

3.3.4. Without Downstream Foundation Contribution

A scenario wherein the downstream wedge contribution (Figure 4) was not considered was also evaluated to assess the influence of the concrete–rock interface strength properties for a less complex failure scenario. Two hypotheses for the concrete–rock strength properties were considered:

(i) The reference contact strength parameters defined in Table 3;

(ii) Adopting the strength properties defined in Table 7 for both the concrete–concrete and concrete–rock, which are the usual ranges for dam concrete [22].

Table 9 shows the numerically predicted shear sliding safety factors for an overtopping scenario obtained for the six adopted dam–foundation systems. Also presented are the percentages relative to the similar scenarios with the wedge contribution (Tables 5a and 8b). As expected, the predicted safety factors without the wedge contribution are lower than those predicted with the wedge presence, which obviously increases the complexity of the failure mode. Notably, the safety factor reduction associated with a less complex failure mode mostly associated with shear sliding is more noticeable for lower concrete–rock strength properties (Table 3), assuming an elastic foundation.

Table 9. Overtopping scenario—safety factors—without wedge contribution.

(a) Concrete–rock with the reference contact properties defined in Table 3 [1]

Foundation Behavior	Approach	Dam Model					
		15-reg	**15-dip**	**30-reg**	**30-dip**	**60-reg**	**60-dip**
E	UCP	2.60 (−29.1)	3.00 (−18.2)	2.00 (−38.8)	2.00 (−40.0)	1.70 (−43.3)	1.63 (−45.6)
	CP	2.33 (−18.6)	2.33 (−18.6)	1.80 (−30.8)	1.80 (−32.5)	1.57 (−35.6)	1.53 (−36.1)
	CP-FP	2.73 (−4.7)	2.33 (−18.6)	1.80 (−30.8)	1.80 (−30.8)	1.57 (−35.6)	1.53 (−36.1)
B	UCP	3.40 (−13.6)	2.60 (−31.6)	2.73 (−10.9)	2.33 (−23.9)	2.20 (−20.5)	2.10 (−23.2)
	CP	3.00 (−11.8)	2.47 (−17.8)	2.40 (−5.3)	2.07 (−20.5)	1.70 (−26.1)	1.93 (−19.4)
	CP-FP	3.00 (−11.8)	2.47 (−17.8)	2.60 (−9.3)	2.07 (−20.5)	2.17 (−5.8)	1.97 (−19.2)

(b) Concrete–rock and concrete–concrete with properties in Table 7 (Cc) [2]

Foundation Behavior	Approach	Dam Model					
		15-reg	**15-dip**	**30-reg**	**30-dip**	**60-reg**	**60-dip**
E	UCP	4.73 (−5.3)	4.60 (−8.0)	2.67 (−27.3)	2.73 (−26.8)	1.70 (−44.0)	2.00 (−33.3)
	CP	4.33 (−5.8)	4.20 (−6.0)	2.47 (−14.0)	2.47 (−15.9)	1.57 (−38.2)	1.77 (−29.3)
	CP-FP	4.87 (−7.6)	4.73 (−5.3)	2.80 (−6.7)	2.87 (−6.5)	1.57 (−38.2)	1.77 (−29.3)
B	UCP	4.73 (−23.7)	2.60 (−33.9)	3.40 (−12.1)	2.40 (−29.4)	2.67 (−7.0)	2.20 (−25.0)
	CP	4.20 (−16.0)	2.47 (−21.3)	3.13 (−9.6)	2.13 (−25.6)	2.33 (−5.4)	2.00 (−22.1)
	CP-FP	4.20 (−16.0)	2.47 (−21.3)	3.40 (−13.6)	2.13 (−25.6)	2.53 (−9.5)	2.00 (−22.1)

[1] The differences to the safety factors presented in Table 5a, in percentages, are shown in brackets with the wedge contribution for similar concrete–rock and concrete–concrete contact strength properties. [2] The differences to the safety factors presented in Table 8b, in percentages, are shown in brackets with the wedge contribution for similar concrete–rock and concrete–concrete contact strength properties.

As shown, for both concrete–rock contact strength property hypotheses with an elastic foundation, the predicted safety factors for the regular foundation geometry for the majority of the cases are lower than those predicted with a brittle foundation. This is related to the fact that with a brittle foundation, near the upstream heel, the nearby foundation blocks open, and the stress distribution along the dam–foundation interface is slightly influenced, which favors the brittle foundation scenario for loading amplification simulation.

For the reference concrete–rock strength properties (Table 3), the CP-FP approach always predicted a safety factor equal to or higher than that predicted with the CP approach, and for the cases where the CP-FP predicted a higher safety factor, the predicted increase compared with the CP approach was significantly higher than that obtained with the wedge presence hypothesis (Section 3.3.1). A similar trend occurred when adopting the contact strength properties in Table 7, where the CP-FP approach even led to more cases where the associated safety factor was higher than the safety factor predicted with the CF approach. As expected, without the wedge consideration, the failure mode was more influenced by the water pressures and stress distribution in the vicinity of the dam foundation.

Figure 15 shows the predicted failure modes for the CP approach for the 60 m high dam for regular and irregular geometries both for an elastic foundation and a brittle foundation. The failure modes predicted with the CP-FP approach are similar to those predicted with the CP approach, where seepage occurred from the onset of the safety factor calculation, and the failure modes obtained with the UCP approach, where the water pressures were not affected by the water height increase, also have similarities to the CP failure modes for all the tested cases.

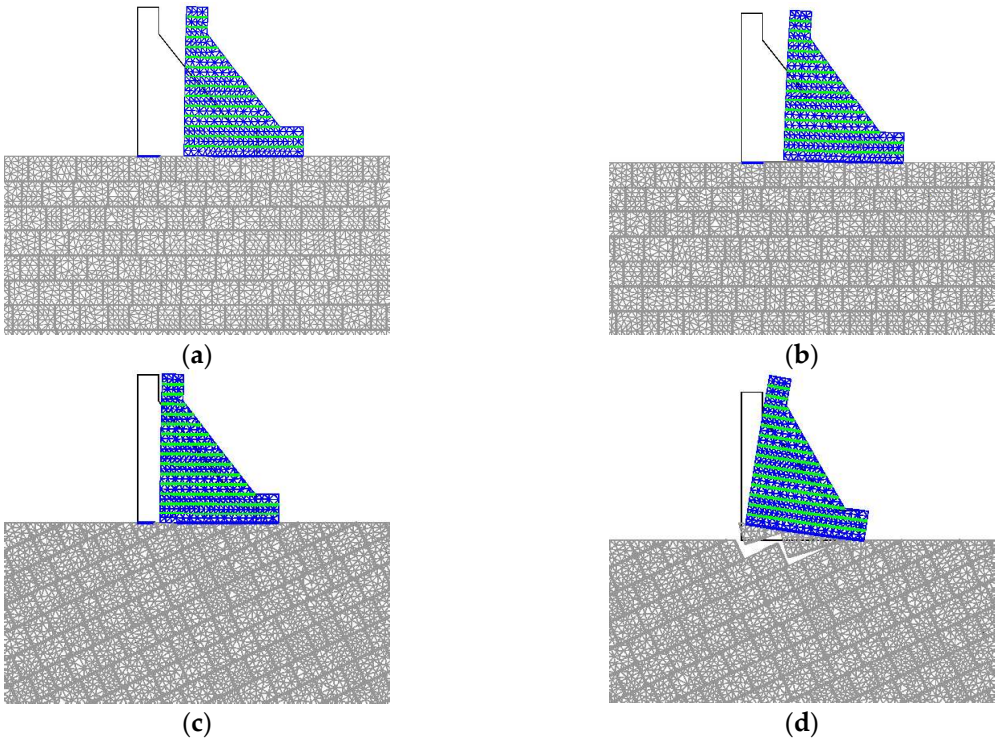

Figure 15. Failure modes associated with the Dam 60-reg and Dam 60-dip hydromechanical discontinuum models of the dam–foundation system (100× amplification factor). (**a**) Dam 60-reg CP (E); (**b**) Dam 60-reg CP (B); (**c**) Dam 60-dip CP (E); (**d**) Dam 60-dip CP (B).

Figure 15 shows that the influence of the foundation behavior on the failure mode is very noticeable for the irregular foundation geometry, where for an elastic foundation, the failure mode is mainly due to sliding along the dam–foundation interface, whereas for a brittle foundation, the failure mode also includes the rock blocks beneath the dam, and the sliding is coupled with rotation along the downstream toe of the dam. For the regular geometry, the failure mode difference is less noticeable, but the foundation behavior influence can also be identified. For a brittle foundation, there is a more evident rotation around the downstream toe in the failure mode. Similar behaviors were recorded for the 15 m and 30 m high dams.

3.4. Modeling Limitations and Future Developments

In the numerical study presented in this work, the water pressures upstream from the dam were gradually increased until failure, although overtopping was not directly simulated. A real overtopping scenario requires the development of fluid models using, for example, the Smooth Particle Hydrodynamics (SPH) method [59–62] or the Particle Finite Element Method (PFEM) [63]. A fluid model can be straightforwardly coupled with the proposed hydromechanical approach: the fluid would interact mechanically with the mechanical model (simulating both the dam and the foundation) and hydraulically with the proposed hydraulic model by setting the corresponding pressure boundary conditions.

In this work, the hydraulic parameters were within the range of the parameters adopted in [42,55], which have been shown to predict the observed hydraulic behavior of a Portuguese gravity dam. For a given dam, additional in situ testing may need to be carried out to properly calibrate the hydraulic parameters following the methodology proposed in [55,64]. Additionally, the hydraulic response predicted with the hydromechanical coupled model should be in good agreement with the monitored response of the operational dam under analysis.

Regarding the concrete–concrete and concrete–rock strength parameters, in this work, the tensile strength-associated properties followed the experimental results presented in [24]. For a new dam, it is important to define these properties (tensile/cohesion) for both materials and interfaces during construction. For a dam under operation, it is fundamental to set these properties by carrying out in situ testing and/or by comparing the numerical results with the known monitored behavior. The thermal state and possible aging or leakage effect need to be considered when defining the interfaces' elastic and strength properties.

The novel integrated methodology presented here for the safety assessment of concrete dams, which adopts a coupled hydromechanical interaction, follows a discrete representation of the foundation discontinuities and considers softening-based constitutive laws. This methodology is presently being adopted (i) to assess stability under seismic loading, for which the model has already been validated using simplified material models [43], and (ii) to assess the influence of the permeability heterogeneity and pre-existing damage distribution on the predicted safety factors. The proposed methodology can also be straightforwardly used to assess the damage caused by explosions (war- or terrorist-related) in an integrated way only requiring the implementation of the explosive loading [65].

In this study, the concept of the overall safety factor was used. This concept has some shortcomings, and the International Commission on Large Dams (ICOLD) is evaluating probability approaches, which allow for the consideration of uncertainties. Some attempts have been made to use the semi-probabilistic approach in the safety assessment of concrete gravity dams [33–35], as prescribed in the Eurocodes for geotechnical and structural design. However, dam–foundation systems are special structures, such as tunnels, foundations of nuclear power plants and offshore structures, and for these types of structures, probability approaches are not yet routinely used. It should be highlighted that semi-probabilistic approaches need to consider hydromechanical coupling and realistic material responses, as proposed in this work.

Further work is underway to apply the recently proposed 3D hydromechanical algorithm in the stability assessment scenario of arch dams for different foundation fracture geometries, where the nonlinearity of the dam body is expected to be even more relevant to the prediction of the correct complex failure modes.

A hybrid analysis model that adopts a particle model based on the discrete element method [40,43] in the vicinity of the dam–foundation interface is also being pursued. This will allow for a more accurate representation of the dam–foundation area of influence, considering more complex nonlinear interactions and pre-existing microcracking.

4. Conclusions

An explicit time-stepping discontinuum hydromechanical coupled algorithm, Parmac-2D-Fflow, was used to evaluate the safety of gravity dams considering various dam heights, foundation geometries and behaviors, and concrete–rock strength properties.

As shown, the strength reduction method commonly used in concrete gravity dam design is overly simplistic. The strength reduction methodology fails to account for the actual material behavior of both the concrete and dam foundation, resulting in excessively conservative safety factors. Additionally, the predicted strength reduction safety factors are not significantly influenced by the dam height, the foundation geometry and behavior or the real concrete–rock and concrete–concrete interface behavior. The strength reduction approach oversimplifies the failure modes, predicting only shear sliding failure, even in scenarios involving a downstream wedge within the rock mass.

The results presented, with the wedge and without the wedge contribution, show that the safety assessment of gravity dams should be conducted using a coupled hydromechanical model that (i) incorporates accurate material properties; (ii) considers the foundation geometry and behavior; (iii) follows a load amplification approach. An initially impervious dam–foundation interface should also be considered, as this represents a more realistic scenario. Additionally, accounting for nonlinearity within the dam body may be crucial for same cases, as neglecting it may lead to overestimated safety factors.

For the results presented with the reference model concrete–rock contact strength properties and for different fracture energy scenarios and contact strength scenarios, the following was found:

- The UCP approach always leads to higher safety factors than those obtained with a coupled approach (CP and CP-FP), which is non-conservative. The UCP approach may also predict incorrect failure modes, which may affect the correct retrofitting interventions. For this reason, it is important to carry out a coupled hydromechanical analysis;
- The safety factor should preferably be defined using the CP-FP approach, which considers the seepage at the dam–foundation interface from the onset of the calculation. In the CP-FP approach, cracking only started to occur at the concrete–rock interface for water levels closer to the maximum water level value for which the dam remains stable. This sudden increase and propagation led, in some cases, to safety factors slightly lower than those predicted with the CP approach.
- The results show that, contrary to the expected, it is possible to obtain safety factors with a brittle foundation higher than those predicted with an elastic foundation. If the proper in situ behavior is not known in advance, the safety factors should be defined following parametric studies;
- If the foundation discontinuities favor the failure mode, its influence on the predicted safety factor is noticeable. For this reason, the geologic characterization is of the upmost importance;
- The parametric studies show that the concrete–rock interface should preferably have a high value of fracture energy or, ideally, higher tensile and cohesion strengths and high associated fracture energy, otherwise the differences in the CP and in the CP-FP predictions are not noticeable;
- During construction, it may be sufficient to characterize the concrete–rock interface only through strength parameter definition (tensile/cohesion), as the results indicate that with a brittle concrete–rock model, the predicted safety factors are always conservative when compared with those that consider the fracture energy.

When compared with the strength reduction method or an overload approach following the UCP approach, the proposed overload approach that follows either the CP or CP-FP

approach predicts more realistic failure modes and, for this reason, has the potential to be used to identify weak structural interfaces/zones that may require reinforcement measures.

Author Contributions: Conceptualization, N.M.A. and M.L.B.F.; methodology, N.M.A. and M.L.B.F.; software, N.M.A.; validation, N.M.A., M.L.B.F. and S.O.; writing—original draft preparation, N.M.A. and M.L.B.F.; writing—review and editing, N.M.A., M.L.B.F. and S.O.; supervision, N.M.A. and M.L.B.F.; project administration, N.M.A. and M.L.B.F. All authors have read and agreed to the published version of the manuscript.

Funding: This research received no external funding.

Data Availability Statement: The original contributions presented in this study are included in the article, and further inquiries can be directed to the corresponding author.

Acknowledgments: The study presented here is part of the research project StepDam: A step forward for the ability to anticipate and prevent failures of concrete dam foundations (Proc. 0403/1102/24145, included in LNEC's Research and Innovation Plan 2021–2027).

Conflicts of Interest: The authors declare no conflicts of interest.

Abbreviations

The following abbreviations are used in this manuscript:

B	Brittle behavior
BL	Bilinear vectorial softening contact model
CP	Coupled approach
CP-FP	CP taking into account fracture propagation at the dam–foundation interface
DDA	Discontinuous deformation analysis
DEM	Discrete element method
E	Elastic behavior
FDEM	Combined finite–discrete element method
FEM	Finite element method
HN	Hydraulic node
ICOLD	International Commission on Large Dams
JE	Joint element
P	Pressure on the HNs
PFEM	Particle finite element method
Q	Discharge in seepage channel
SC	Seepage channel
SPH	Smooth particle hydrodynamics
THM	Thermal–hydromechanical coupled model
UCP	Uncoupled approach
XFEM	Extended finite element method

References

1. ASDSO. *Dam Failure and Incident Investigation Guide*, Version 2.0; Updated March 2021; ASDSO: Lexington, KY, USA, 2021.
2. Vulliet, F.; Ftima, M.B.; Léger, P. Stability of cracked concrete hydraulic structures by nonlinear quasi-static explicit finite element and 3D limit equilibrium methods. *Comput. Struct.* **2017**, *184*, 25–35. [CrossRef]
3. Pereira, R.; Batista, A.L.; Neves, L.C.; Lemos, J.V. Deduction of ultimate equilibrium limit states for concrete gravity dams keyed into rock mass foundations based on large displacement analysis. *Structures* **2022**, *38*, 1180–1190. [CrossRef]
4. Cammarata, G.; Fidelibus, C.; Cravero, M.; Barla, G. The hydro-mechanically coupled response of rock fractures. *Rock Mech. Rock Eng.* **2007**, *40*, 41–61. [CrossRef]
5. Callari, C.; Fois, N.; Cicivelli, R. The role of hydro-mechanical coupling in the behaviour of dam-foundation system. In Proceedings of the Computational Mechanics, WCCM VI in Conjunction with APCOM'04, Beijing, China, 5–10 September 2004.
6. Alonso, E.E.; Zandarín, M.T.; Olivella, S. Joints in unsaturated rocks: Thermo-hydro-mechanical formulation and constitutive behaviour. *J. Rock Mech. Geotech. Eng.* **2013**, *5*, 200–213. [CrossRef]

7. Lopez, P.; Thoraval, A.; Buzzi, O.; Rahmani, I.; Boulon, M. Advances in constitutive modelling of jointed rock hydro mechanical interactions at laboratory scale. In Proceedings of the 18 ème Congrès Français de Mécanique, Grenoble, France, 27–31 August 2007.
8. Li, Y.; Oh, J.; Mitra, R.; Hebblewhite, B. A constitutive model for a laboratory rock joint with multi-scale asperity degradation. *Comput. Geotech.* **2016**, *72*, 143–151. [CrossRef]
9. Liu, Y.; Huang, D.; Zhao, B.; Wang, C.; Cen, D. Nonlinear creep behavior and viscoelastic-plastic constitutive model of rock-concrete composite mass. *Adv. Civ. Eng.* **2020**, *2020*, 9059682. [CrossRef]
10. Zandarin, M.T.; Alonso, E.; Olivella, S. A constitutive law for rock joints considering the effects of suction and roughness on strength parameters. *Int. J. Rock Mech. Min.* **2013**, *60*, 333–344. [CrossRef]
11. Farinha, M.L.B.; Azevedo, N.M.; Schclar Leitão, N.A.; Rocha de Almeida, J.; Oliveira, S. Sliding stability assessment of concrete dams using a 3D discontinuum hydromechanical model following a discrete crack approach. *Geotechnics* **2022**, *2*, 133–157. [CrossRef]
12. Yan, C.; Zheng, H. A two-dimensional coupled hydro-mechanical finite-discrete model considering porous media flow for simulating hydraulic fracturing. *Int. J. Rock Mech. Min.* **2016**, *88*, 115–128. [CrossRef]
13. Yan, C.; Jiao, Y.Y.; Zheng, H. A fully coupled three-dimensional hydro-mechanical finite discrete element approach with real porous seepage for simulating 3D hydraulic fracturing. *Comput. Geotech.* **2018**, *96*, 73–89. [CrossRef]
14. Yan, C.; Xie, X.; Ren, Y.; Ke, W.; Wang, G. A FDEM-based 2D coupled thermal-hydro-mechanical model for multiphysical simulation of rock fracturing. *Int. J. Rock Mech. Min.* **2022**, *149*, 104964. [CrossRef]
15. Yan, C.; Zhao, Z.; Yang, Y.; Zheng, H. A three-dimensional thermal-hydro-mechanical coupling model for simulation of fracturing driven by Multiphysics. *Comput. Geotech.* **2023**, *155*, 105162. [CrossRef]
16. Geomechanica Inc. *Irazu 2D Geomechanical Simulation Software, V510*; Theory Manual; Geomechanica Inc.: Toronto, ON, Canada, 2022.
17. Sharafisafa, M.; Aliabadian, Z.; Sato, A.; Shen, L. Coupled thermo-hydro-mechanical simulation of hydraulic fracturing in deep reservoirs using finite-discrete element method. *Rock Mech. Rock Eng.* **2023**, *56*, 5039–5075. [CrossRef]
18. Deng, Y.; Wang, D.; Jin, Y.; Xia, Y. A fully coupled hydro-mechanical approach for multi-fracture propagation simulations. *Energies* **2023**, *16*, 1601. [CrossRef]
19. Zhang, Q.-H.; Shi, G.-H. Verification of a DDA-based hydro-mechanical model and its application to dam foundation stability analysis. *Int. J. Rock Mech. Min.* **2021**, *138*, 104627. [CrossRef]
20. Zhang, W.; Li, H.; Shi, D.; Shen, Z.; Zhao, S.; Guo, C. Determination of safety monitoring indices for roller-compacted concrete dams considering seepage–stress coupling effects. *Mathematics* **2023**, *11*, 3224. [CrossRef]
21. Serra, C.; Batista, A.L.; Azevedo, N. Monteiro, Dam and wet-screened concrete creep in compression: In situ experimental results and creep strains prediction using model B3 and composite models. *Mater. Struct.* **2016**, *49*, 4831–4851. [CrossRef]
22. Serra, C.; Batista, A.L.; Azevedo, N.M.; Custódio, J. Prediction of dam concrete compressive and splitting tensile strength based on wet-screened concrete test results. *J. Mater. Civ. Eng.* **2017**, *29*, 1–37. [CrossRef]
23. Electric Power Research Institution. *Uplift Pressures, Shear Strengths, and Tensile Strengths for Stability Analysis of Concrete Gravity Dams*; Electric Power Research Institution: Palo Alto, CA, USA, 1992.
24. Dong, W.; Wu, Z.; Zhou, X. Fracture mechanisms of rock-concrete interface: Experimental and numerical. *J. Eng. Mech.* **2016**, *142*, 04016040. [CrossRef]
25. Dong, W.; Wu, Z.; Zhou, X.; Wang, N.; Kastiukas, G. An experimental study on crack propagation at rock-concrete interface using digital image correlation technique. *Eng. Fract. Mech.* **2017**, *171*, 50–63. [CrossRef]
26. Dong, Z.; Lin, T.; Tang, S.; Lang, Y.; Yuan, R.; Heng, S. Mechanical properties and failure mechanism of concrete-granite composite specimens under compression load. *Constr. Build. Mater.* **2024**, *435*, 136768. [CrossRef]
27. FERC. *Gravity Dams*; Federal Energy Regulatory Commission, Division of Dam Safety and Inspections: Washington, DC, USA, 2016; Chapter 3.
28. Hellgren, R.; Malm, R.; Ansell, A. Progressive failure analysis of a concrete dam anchored with passive rock bolts. *Infrastructures* **2020**, *5*, 28. [CrossRef]
29. USACE. *Gravity Dam Design*; USACE: Springfield, VA, USA, 1995.
30. European Club of ICOLD. *Sliding Safety of Existing Gravity Dams—Final Report*; European Club of ICOLD: Chatou, France, 2004.
31. Li, W.; Wu, W.; Zhang, J. Numerical stability analysis of the dam foundation under complex geological conditions at great depth: A case study of Kala Hydropower Station, China. *Front. Phys.* **2022**, *9*, 808840. [CrossRef]
32. Bao, T.F.; Xu, M.; Chen, L. Stability analysis of concrete gravity dam foundation based on catastrophe model of plastic strain energy. *Procedia Eng.* **2012**, *28*, 825–830. [CrossRef]
33. Haghighi, A.; Ayati, A.H. Stability analysis of gravity dams under uncertainty using the fuzzy sets theory and a many-objective GA. *J. Intell. Fuzzy Syst.* **2016**, *30*, 1857–1868. [CrossRef]

34. Pereira, R.; Lamas, L.; Muralha, J. Sliding stability analyses of a rock slope using deterministic, semi-probabilistic and probabilistic methods. In *IOP Conference Series: Earth and Environmental Science*; IOP Publishing Ltd.: Bristol, UK, 2021. [CrossRef]
35. Wang, D.; Lu, X.; Zheng, C.; Gong, K.; Pan, L.; Pei, L.; Zhao, Z. Influence analysis of material parameter uncertainties on the stability safety factor of concrete gravity dams: A probabilistic method. *Buildings* **2024**, *14*, 2435. [CrossRef]
36. Malm, R. Guideline for FE Analyses of Concrete Dams, Stockholm, Sweden. 2016. Available online: www.energiforsk.se (accessed on 3 March 2024).
37. Enzell, J.; Nordström, E.; Sjölander, A.; Ansell, A.; Malm, R. Physical model tests of concrete buttress dams with failure imposed by hydrostatic water pressure. *Water* **2023**, *15*, 3627. [CrossRef]
38. Zhu, H.-H.; Yin, J.-H.; Dong, J.-H.; Zhang, L. Physical modelling of sliding failure of concrete gravity dam under overloading condition. *Geomech. Eng.* **2010**, *2*, 89–106. [CrossRef]
39. Azevedo, N.M.; Farinha, M.L.B. A hydromechanical model for the analysis of concrete gravity dam foundations. *Geotecnia* **2015**, *133*, 5–33. [CrossRef]
40. Azevedo, N.M.; Candeias, M.; Gouveia, F. A Rigid particle model for rock fracture following the Voronoi tessellation of the grain structure: Formulation and validation. *Rock Mech. Rock Eng.* **2015**, *48*, 535–557. [CrossRef]
41. Enzell, J.; Ulfberg, A.; Sas, G.; Malm, R. Post-peak behavior of concrete dams based on nonlinear finite element analyses. *Eng. Fail. Anal.* **2021**, *130*, 105778. [CrossRef]
42. Farinha, M.L.B.; Azevedo, N.M.; Candeias, M. Small displacement coupled analysis of concrete gravity dam foundations: Static and dynamic Conditions. *Rock Mech. Rock Eng.* **2017**, *50*, 439–464. [CrossRef]
43. Azevedo, N.M.; Lemos, J.V.; Almeida, J.R. A discrete particle model for reinforced concrete fracture analysis. *Struct. Eng. Mech.* **2010**, *36*, 343–361. [CrossRef]
44. Itasca. *UDEC—Universal Distinct Element Code*, Version 4.0; Itasca: Minneapolis, MN, USA, 2004.
45. Rampal, A.; Halder, P.; Manna, B.; Sharma, K.G. Static and coupled hydro-mechanical analyses of concrete gravity dam resting on jointed rock foundation. *Geotech. Geol. Eng.* **2020**, *38*, 4111–4127. [CrossRef]
46. Goodman, R.; Taylor, R.; Brekke, T. A model for the mechanics of jointed rock. *J. Soil Mech. Found. Div. ASCE* **1968**, *94*, 637–659. [CrossRef]
47. Hohberg, J. *A Joint Element for the Nonlinear Dynamic Analysis of Arch Dams*; ETH, Institute of Structural Engineering: Zurich, Switzerland, 1992.
48. Lemos, J.V. Representation of rock discontinuities in safety analysis of large dams. In *Rock Engineering and Rock Mechanics: Structures in and on Rock, Proceedings of the 2014 ISRM European Rock Mechanics Symposium (EUROCK 2014), Vigo, Spain, 27–29 May 2014*; Alejano, R., Perucho, Á, Olalla, C., Jiménes, R., Eds.; Taylor and Francis Group: London, UK, 2014; ISBN 978-1-138-00149-7.
49. Louis, C.A. Study of Groundwater Flow in Jointed Rock and Its Influence on the Stability of Rock Masses. Ph.D. Thesis, Imperial College of Science and Technology, London, UK, 1969.
50. Louis, C.; Maini, Y.N. Determination of in situ hydraulic parameters in jointed rock. In Proceedings of the 2nd International Congress on Rock Mechanics, Belgrade, Serbia, 21–26 September 1970; pp. 235–245.
51. Snow, D.T. A Parallel Plate Model of Fractured Permeable Media. Ph.D. Dissertation, University of California, Berkeley, CA, USA, 1965.
52. Bear, J. *Dynamics of Fluids in Porous Media*; Dover Publications, Inc.: New York, NY, USA, 1988.
53. Zhong, H.; Ooi, E.T.; Song, C.; Ding, T.; Lin, G.; Li, H. Experimental and numerical study of the dependency of interface fracture in concrete–rock specimens on mode mixity. *Eng. Fract. Mech.* **2014**, *124*, 287–309. [CrossRef]
54. Dong, W.; Yang, D.; Zhang, B.; Wu, Z. Rock-concrete interfacial crack propagation under mixed mode I-II fracture. *J. Eng. Mech.* **2018**, *144*, 04018039. [CrossRef]
55. Farinha, M.L.B. Hydromechanical Behaviour of Concrete Dam Foundations, Insitu Tests and Numerical Modelling. Ph.D. Thesis, Technical University of Lisbon, Lisbon, Portugal, 2010.
56. Farinha, M.L.B.; Lemos, J.; Neves, E.M. Analysis of foundation sliding of an arch dam considering the hydromechanical behavior. *Front. Struct. Civ. Eng.* **2012**, *6*, 35–43. [CrossRef]
57. FERC. *Dam Safety Performance Monitoring Program*; FERC: Washington, DC, USA, 2005; Chapter 14.
58. ICOLD. *Guidelines for Use of Numerical Models in Dam Engineering, Paris*. 2013. Available online: www.icold-cigb.net (accessed on 15 February 2025).
59. Zhang, J.; Wang, B.; Li, H.; Zhang, F.; Wu, W.; Hu, Z.; Deng, C. Progressive Dam-failure assessment by smooth particle hydrodynamics (SPH) method. *Water* **2023**, *15*, 3869. [CrossRef]
60. Su, Z.; Wang, S.; Li, D.; Sheng, J.; Wu, W. SPH–DEM modeling overtopping failure of earthfill dams. *Acta Geotech.* **2024**, *19*, 953–970. [CrossRef]
61. Blanc, T.; Pastor, M. Towards sph modelling of failure problems in geomechanics: A fractional step taylor-sph model. *Eur. J. Environ. Civ. Eng.* **2011**, *15*, 31–49. [CrossRef]

62. Xu, X.; Jiang, Y.L.; Yu, P. SPH simulations of 3D dam-break flow against various forms of the obstacle: Toward an optimal design. *Ocean Eng.* **2021**, *229*, 108978. [CrossRef]
63. Cremonesi, M.; Franci, A.; Idelsohn, S.; Oñate, E. A state of the art review of the Particle Finite Element Method (PFEM). *Arch. Comput. Method E* **2020**, *27*, 1709–1735. [CrossRef]
64. Farinha, M.L.B.; Lemos, J.; Maranha das Neves, E. Numerical modelling of borehole water-inflow tests in the foundation of the Alqueva arch dam. *Can. Geotech. J.* **2010**, *48*, 72–88. [CrossRef]
65. Huo, W. Blast-Resistance and damage behavior of underwater explosion for concrete gravity dam considering concrete strength partition. *Buildings* **2023**, *13*, 2237. [CrossRef]